Supporting Information for

Tuneable CO_2 Binding Enthalpies by Redox Modulation of an Electroactive MOF-74 Framework

Patrick W. Doheny,[a] Ravichandar Babarao,[b] Cameron J. Kepert[a*] and Deanna M. D'Alessandro[a*]

[a] School of Chemistry, The University of Sydney, New South Wales, 2006 Australia.

[b] School of Science, Royal Melbourne Institute of Technology (RMIT University), Victoria, 3001 Australia.

[*] Corresponding author's phone: +61 2 93513777; email: deanna.dalessandro@sydney.edu.au; cameron.kepert@sydney.edu.au

Additional Synthetic Details

***N,N'*-bis(4-carboxy-3-hydroxyphenyl)-1,4,5,8-naphthalenetetracarboxylic Acid Diimide (H_4DSNDI) Ligand.** The DSNDI ligand was synthesised using a modified form of the procedure reported by Saha.[1] 1,4,5,8-naphthalenetetracarboxylic dianhydride (2.68 g, 10 mmol) and 4-aminosalicylic acid (4.60 g, 30 mmol) were suspended in a mixture of dry DMF (15 mL) and trimethylsilyl chloride (6.4 mL, 50 mmol) and refluxed at 153 °C overnight. The mixture was cooled to room temperature at which point DMF (15 mL) was added to the mixture which was stirred and then filtered. The resulting crude was then was washed successively with cold DMF followed by H_2O and then MeOH before drying under vacuum to yield the target compound as a yellow solid (1.72 g, 3.19 mmol, 32%). ^{1}H NMR (d_6-DMSO, 200 MHz): δ 8.73 (s, 4H), 7.88 (d, $^3J_{H\text{-}H}$ = 8.1 Hz, 2H), 7.15 (s, 2H), 7.07 (dd, $^3J_{H\text{-}H}$ = 8.5 Hz, $^4J_{H\text{-}H}$ = 7.2 Hz, 2H) ppm. ^{13}C{^{1}H} NMR (d_6-DMSO, 75 MHz): 206.5, 171.4, 162.6, 161.4, 141.8, 130.3, 127.0, 126.7, 120.2, 118.1, 113.3. ESI-MS (ESI$^+$, MeOH) *m*/*z* calculated for $C_{28}H_{14}N_2O_{10}$ $[M+H]^+$: 538.06, Found: 539.08 (100%). Elemental Analysis: Found: C 62.33%, H 3.64%, N 6.63%; Calculated for $C_{28}H_{14}N_2O_{10}$: C 62.46%, H 2.62%, N 5.20%.

Single crystals of the H_4DSNDI ligand were obtained from a recrystallisation of the pure solid from DMF to yield yellow plate crystals suitable for characterisation by single crystal X-ray diffraction. Crystallographic data for the H_4DSNDI ligand is given in Table S1 and the corresponding CIF has been deposited with the CSD under the deposition code CCDC 2002851.

A sample of the material for gas sorption analysis was prepared as follows: DMF was exchanged twice a day over the course of three days with MeOH before the MeOH-exchanged material was heated at 80 °C under vacuum for 18 h to yield the activated material. The *de novo* and activated materials were observed

to decompose upon exposure to atmospheric conditions leading to an amorphous phase; thus, the material was kept under solvent at all times and was handled in a glove box under Ar once activated. The retention of structure and crystallinity after both solvent exchange and activation was confirmed using capillary PXRD (Figure S8) prior to gas sorption analysis.

Chemical Reduction of Zn_2(DSNDI). The activated Zn_2(DSNDI) framework (200 mg, 0.30 mmol) was suspended in a solution of lithium naphthalenide (0.1 M in dry THF) and stirred for 2 hrs in a glove box under an argon atmosphere. The solid was then filtered and washed several times with dry THF to remove any residual naphthalenide or naphthalene and dried to yield the chemically reduced framework. The reduced samples were stored under an argon atmosphere prior to analysis.

Additional Instrument Details

Thermal Gravimetric Analysis (TGA). TGA analysis was performed using a TA Instruments Discovery Thermogravimetric Analyser from 25-600 °C at 2 °C min^{-1} under a flow of nitrogen gas (0.1 L min^{-1}).

X-ray Powder Diffraction (PXRD). PXRD measurements of the Zn_2(DSNDI) framework and its chemically reduced analogues were carried out using a PANalytical X'Pert PRO diffractometer equipped with a solid-state PIXcel detector and utilising Cu-Kα (λ = 1.5406 Å) radiation. The samples were loaded into flame-sealed 0.5 mm diameter glass capillaries under solvent (for the pre-activated Zn_2(DSNDI) materials) or an argon atmosphere (for the activated and chemically reduced phases).

Single Crystal X-ray Diffraction of H_4DSNDI. A yellow plate crystal of the H_4DSNDI ligand was mounted using a thin film of Paratone *N* oil on a Rigaku SuperNova, Dual Atlas diffractometer employing monochromated CuKα generated from a sealed X-ray tube. The structure was collected at 100(2) K in a nitrogen gas stream from an Oxford Cryosystems Cryostream with cell constants obtained from a least squares refinement of 7235 reflections located between 3.975 and 72.427 ° 2θ. The data was processed and integrated within CrysAlisPro[2] with a multi-scan empirical absorption correction applied using spherical harmonics within the SCALE3 ABSPACK scaling algorithm.[3] The structure was solved with dual space methods using SHELXT[4] in the monoclinic *P*2/*c* (#13) space group and refined using SHELXL-2018/3[5] within the ShelXle[6] graphical user interface. The DMF within the structure was found to be disordered across two positions with the site occupancy factor refining to 0.54 and 0.46 respectively. The hydroxyl group of the DSNDI ligand was also found to be disordered across two orientations with the occupancy of the first component refining to 0.9 while the second was found to be only a minor component refining to an occupancy of 0.1. With the exception of the hydroxyl O atom of the minor hydroxyl disorder component, all non-hydrogen atoms in the asymmetric unit were refined anisotropically and the hydrogen atoms placed using a riding model with group displacement parameters. Crystallographic data for the H_4DSNDI ligand

is given in Table S1 and the corresponding CIF has been deposited with the CSD under the deposition code CCDC 2002851.

Solution-State UV-Vis-NIR Spectroelectrochemistry of H_4DSNDI. Solution state UV-Vis-NIR spectroelectrochemistry experiments were carried out on a CARY5000 Spectrophotometer equipped with a custom-made quartz optically transparent thin-layer electrochemical (OTTLE) cell fused to a cylindrical quartz compartment. The 0.685 cm pathlength cell contained a platinum gauze working electrode connected to a platinum wire that was wrapped in Teflon. A Pt wire auxiliary electrode and an Ag/Ag^+ *quasi*-reference electrode were encased in separate sintered frits and lowered into the cylindrical body which was filled with electrolyte such that all electrodes were immersed. The cell was capped with a Teflon cap to minimise oxygen diffusion and electrolyte evaporation and the applied potential controlled using an eDAQ e-corder 410 potentiostat. A baseline correction was applied to all spectral data using neat electrolyte after which a 0.41 mmol solution of the analyte was introduced into the cell.

EPR Spectroelectrochemistry. The procedure and cell set-up used were as previously reported for solid-state EPR spectroelectrochemical experiments.[7-9] Briefly, a three electrode set-up consisting of a platinum wire working and auxiliary electrode each with a platinum mesh attached to the ends and a silver wire *quasi*-reference electrode. The wires were coated with Teflon to prevent short-circuiting with the bottom 1 cm of each wire stripped, with the exception of the auxiliary electrode wire that was completely bare. The sample was immobilised on a platinum mesh connected to the end of the platinum wire working electrode and inserted into a cell consisting of a flame-sealed pipette with the exposed wires well separated. The potential was controlled using an eDAQ e-corder 410 potentiostat with 0.1 M $[(n\text{-}C_4H_9)_4N]PF_6$ in dry MeCN supporting electrolyte. Continuous wave X-band EPR spectra were recorded using a Bruker EMXnano spectrometer equipped with a 0.65 T electromagnet with the microwave power and attenuation tuned to prevent signal saturation. The EPR signals obtained were referenced to strong pitch to obtain the *g*-value and spectral simulations were carried out using the Easyspin simulation package.[10]

Solid-State EPR Spectroscopy. Continuous wave X-band EPR measurements were performed using a benchtop Bruker EMXnano spectrometer equipped with a 0.65 T electromagnet. Samples were loaded into quartz EPR tubes and spectra were obtained at room temperature; air sensitive samples were loaded into EPR tubes in a glovebox under argon and capped with septa to prevent any interaction with the atmosphere. The microwave power and attenuation was tuned for each sample to prevent signal saturation. The EPR signals obtained were referenced to strong pitch to obtain the *g*-value and spectral simulations were carried out using the Easyspin simulation package.[10]

Solid-State UV-Vis-NIR Spectroscopy. Solid-state UV-Vis-NIR spectroscopy was performed using a Cary5000 Spectrophotometer equipped with a Harrick Praying Mantis attachment. Solid powdered samples were prepared in a dry $BaSO_4$ background matrix with spectra acquired over a 5000-40000 cm^{-1} energy

range at a scan rate of 6000 cm^{-1}/min. Air sensitive samples were loaded into a Harrick ambient pressure dome accessory equipped with SiO_2 windows under an argon atmosphere. All spectral data is reported as the Kubelka-Munk transform, where $F(R) = (1-R^2)/2R$ (where R is the diffuse reflectance of the sample relative to the $BaSO_4$ baseline).

Inductively Coupled Plasma Mass Spectrometry (ICP-MS). ICP-MS measurements were performed using a Perkin Elmer Nexion 300X. Samples were open digested in concentrated HNO_3 overnight at room temperature before dilution with milliQ water to a 1 ppm - 1 ppb concentration range. Calibration curves were constructed with Cu, Cr, Fe, Co as a mixed standard using a Hamilton autodiluter. Samples and standards were spiked with a standard mix of Sc, Rh and Ir as internal standards. All elements were measured in standard and KED mode (helium gas 5 L/min).

Isosteric Heat of Adsorption Calculations. The isosteric heats of adsorption (Q_{st}) for CO_2 was calculated by applying the Clausius-Clapeyron equation to the CO_2 isotherms of the neutral and chemically reduced materials obtained at 298, 308 and 318 K.

$$(lnP)_N = -(\frac{Q_{st}}{R})(\frac{1}{T}) + C$$

where P is the pressure (in kPa) and N is the quantity adsorbed (in mmol/g) at a given loading, R is the universal gas constant, T is the temperature (in K) and C is a constant.

Simulation Details.

Simulated Annealing: To identify the initial location of lithium cation in the primitive cell of the Zn_2(DSDNI) reduced MOF structure, simulated annealing technique using classical force field as implemented in sorption module in Materials Studio were employed.[11] The framework atoms are kept frozen during simulation. The interactions of lithium−adsorbent and lithium − lithium cations were modelled as a combination of pairwise site−site Lennard-Jones (LJ) and Columbic potentials. The LJ potential parameters of both the framework atoms and the lithium cation are adopted from the universal force field.[12] The charges for the framework atoms were assigned based on the Qeq charges as implemented in Materials Studio package. In the simulated annealing method, the temperature was lowered stepwise, allowing the gas molecule to reach a desirable configuration based on different moves such as rotation, translation, and repositioning with preset probabilities of occurrence. This process of heating and cooling the system was repeated in several heating cycles to find the local minima. Forty heating cycles were performed where the maximum temperature and the final temperature were 10^5 and 100 K, respectively. Similarly, the lowest energy configuration of one CO_2 molecule in both the neutral and the reduced Zn_2(DSDNI) MOF structures were obtained based on the same procedure as described above.

Density Functional Theory Calculations.

Periodic geometric optimization and the static binding energies for CO_2 in neutral and reduced Zn_2(DSDNI) MOF structures were calculated using density functional theory (DFT) as implemented in the software package VASP 5.4.4.[13] It is well known that standard DFT methods based on generalized gradient approximation do not fully account for the dispersion energies of CO_2 with the framework; we implemented dispersion corrections using DFT-D3 method.[14] Electron exchange and correlation were described using the generalized gradient approximation Perdew, Burke, and Ernzerhof form,[15] and the projector-augmented wave potentials were used to treat core and valence electrons.[16] In all cases, we used a plane-wave kinetic energy cutoff of 650 eV and a *k*-point grid of (111) γ-point mesh for sampling the Brillouin zone. The ionic coordinates were relaxed until the Hellman−Feynman ionic forces were less than 0.02 eV/Å and the lattice parameters are kept fixed.

Static binding energies (ΔE) at 0 K in vacuum were calculated using the following expression

$$\Delta E = E_{MOF+\mathrm{CO2}} - E_{MOF} - E_{\mathrm{CO2}}$$

where E_x refers, respectively, to the total energies of the MOF + CO_2 complex, the MOF alone, and the CO_2 molecule respectively.

Table S1. Crystallographic data for H_4DSNDI

Parameter	DSNDI
Empirical formula	$C_{34}H_{28}N_4O_{12}$

Formula weight	684.60
Temperature/K	100(2)
Crystal system	monoclinic
Space group	*P*2/*c*
***a* / Å**	12.9874(5)
***b* / Å**	5.2407(2)
***c* / Å**	22.1191(7)
***α* / °**	90
***β* / °**	95.797(3)
***γ* / °**	90
Volume / Å^3	1497.79(9)
Z	2
ρ_{calc} / g cm^{-3}	1.518
μ / mm^{-1}	0.990
F(000)	712.0
Crystal size / mm^3	0.206 × 0.098 × 0.027
Radiation	CuKα (λ = 1.54178)
2Θ range for data collection / °	6.84 to 153.338
Index ranges	-16 ≤ h ≤ 16, -6 ≤ k ≤ 6, -27 ≤ l ≤ 27
Reflections collected	50747
Independent reflections	3151 [R_{int} = 0.0710, R_{sigma} = 0.0276]
Data / restraints / parameters	3151 / 0 / 265
Goodness-of-fit on F^2	1.041
Final R indexes [I ≥ 2*σ*(I)]	R_1 = 0.0512, wR_2 = 0.1386
Final R indexes [all data]	R_1 = 0.0729, wR_2 = 0.1544
Largest diff. peak / hole / e Å^{-3}	0.32 / -0.20

* $R_1 = \Sigma||F_o| - |F_c||/\Sigma|F_o|$ for $F_o > 2\sigma(F_o)$; $wR_2 = (\Sigma w(F_o^2 - F_c^2)^2/\Sigma(wF_c^2)^2)^{1/2}$ all reflections $w=1/[\sigma^2(F_o^2)+(0.0896P)^2+13.3135P]$ where $P=(F_o^2+2F_c^2)/3$

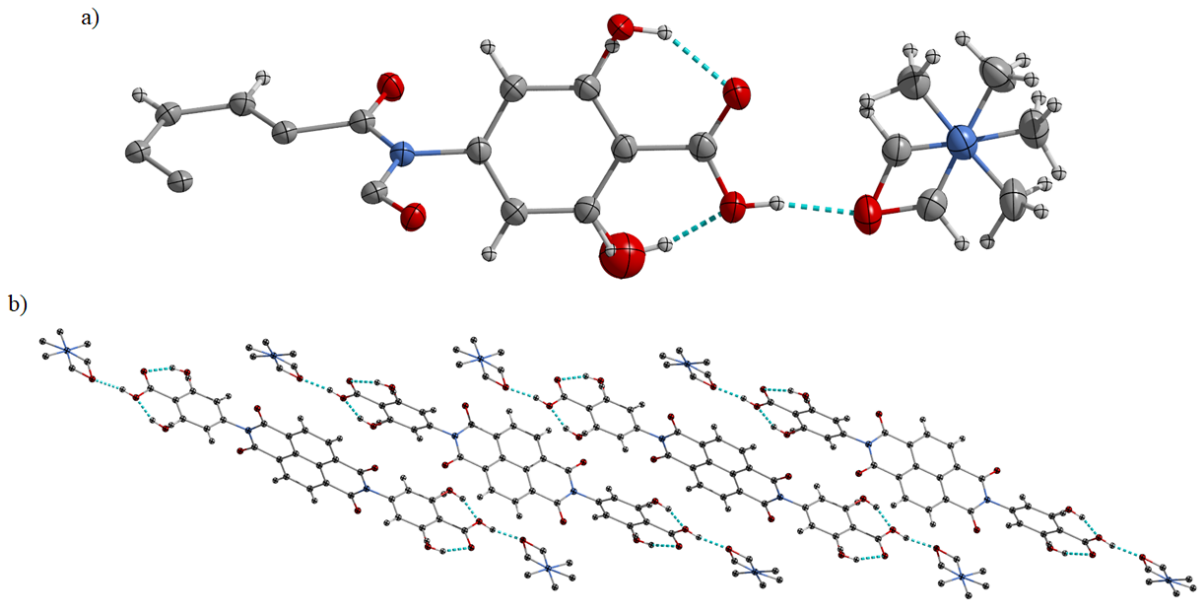

Figure S1. Crystal structure of the DSNDI ligand showing a) the asymmetric unit and b) the crystal structure viewed down the crystallographic *b*-axis showing the hydrogen bonding interactions between the DSNDI and DMF solvent units. The thermal ellipsoids in a) are shown at 50% probability where O = red, N = blue, C = grey, H = white and hydrogen bonds are shown as dashed lines. The hydrogen atoms of the DMF in b) have been omitted for clarity.

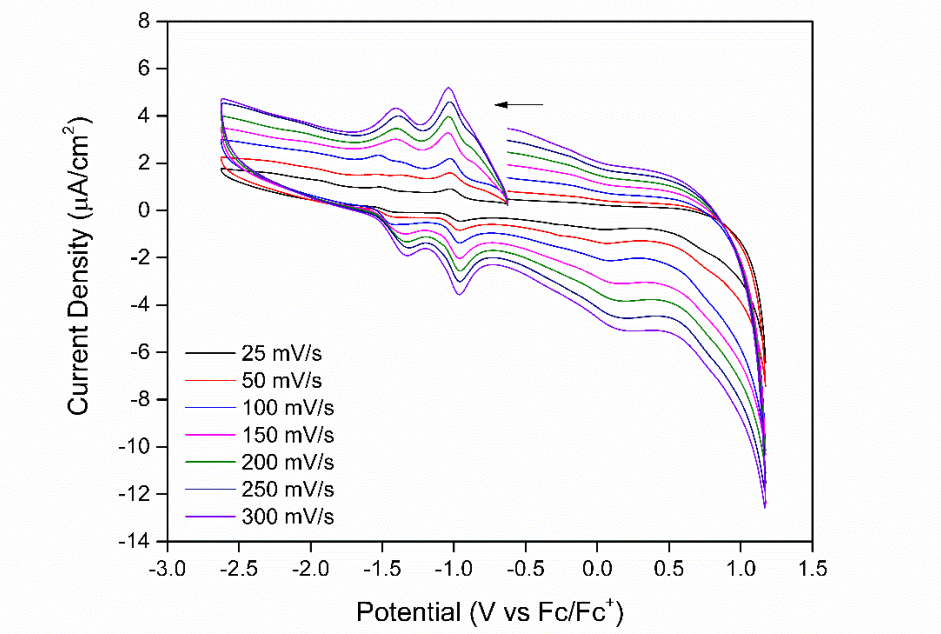

Figure S2. Solution-state cyclic voltammetry of H_4DSDNI in 0.1 M [(*n*-C_4H_9)$_4$N]PF_6/DMF supporting electrolyte at scans rates of 25-250 mV/s. The arrow indicates the direction of the forward scan.

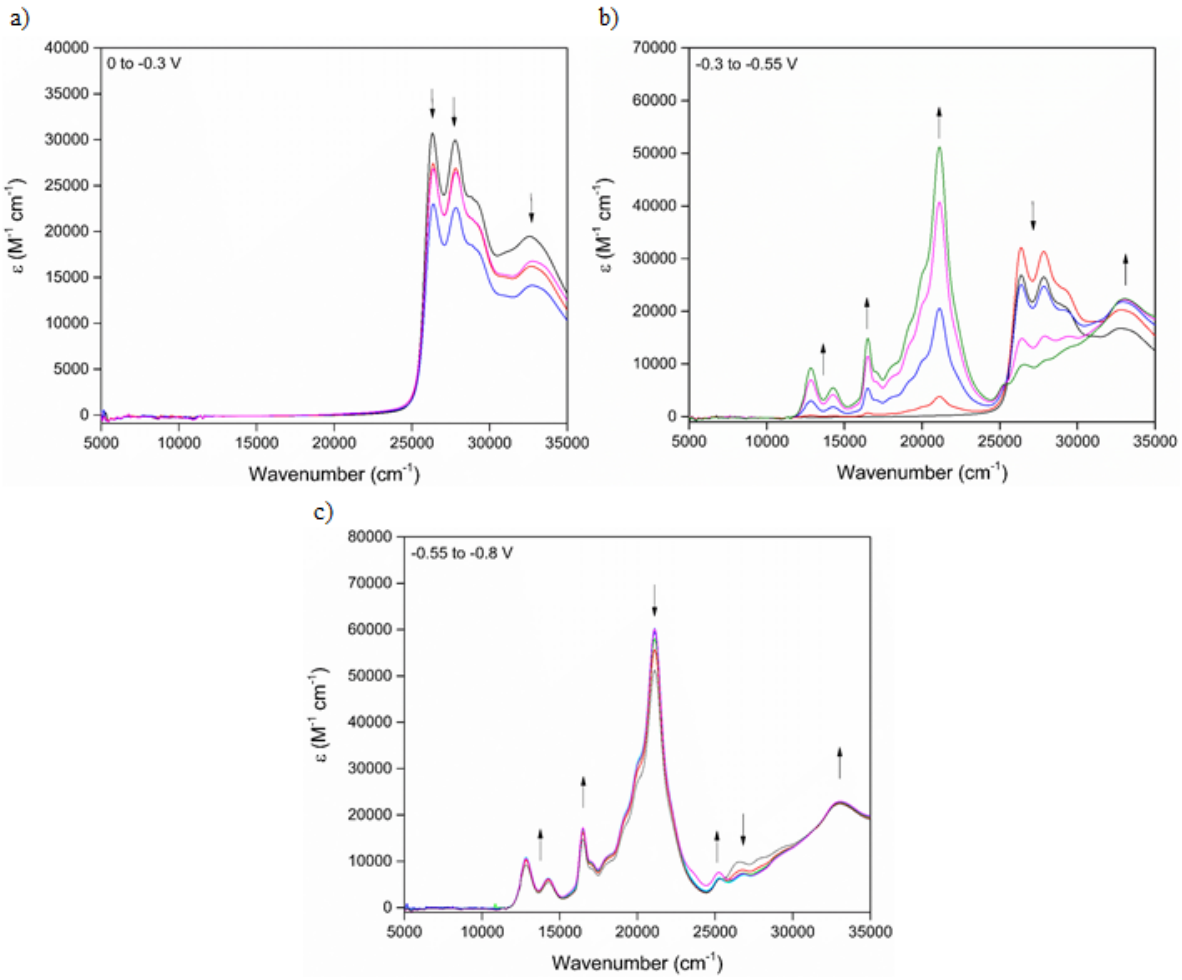

Figure S3. Solution-state UV-Vis-NIR spectroelectrochemistry of the H_4DSNDI ligand in 0.1 M [(*n*-$C_4H_9)_4N]PF_6$/DMF electrolyte over a potential range of a) 0 to -0.3 V, b) -0.3 to -0.55 V and c) -0.55 to -0.8 V showing the formation of the H_4DSNDI radical anion.

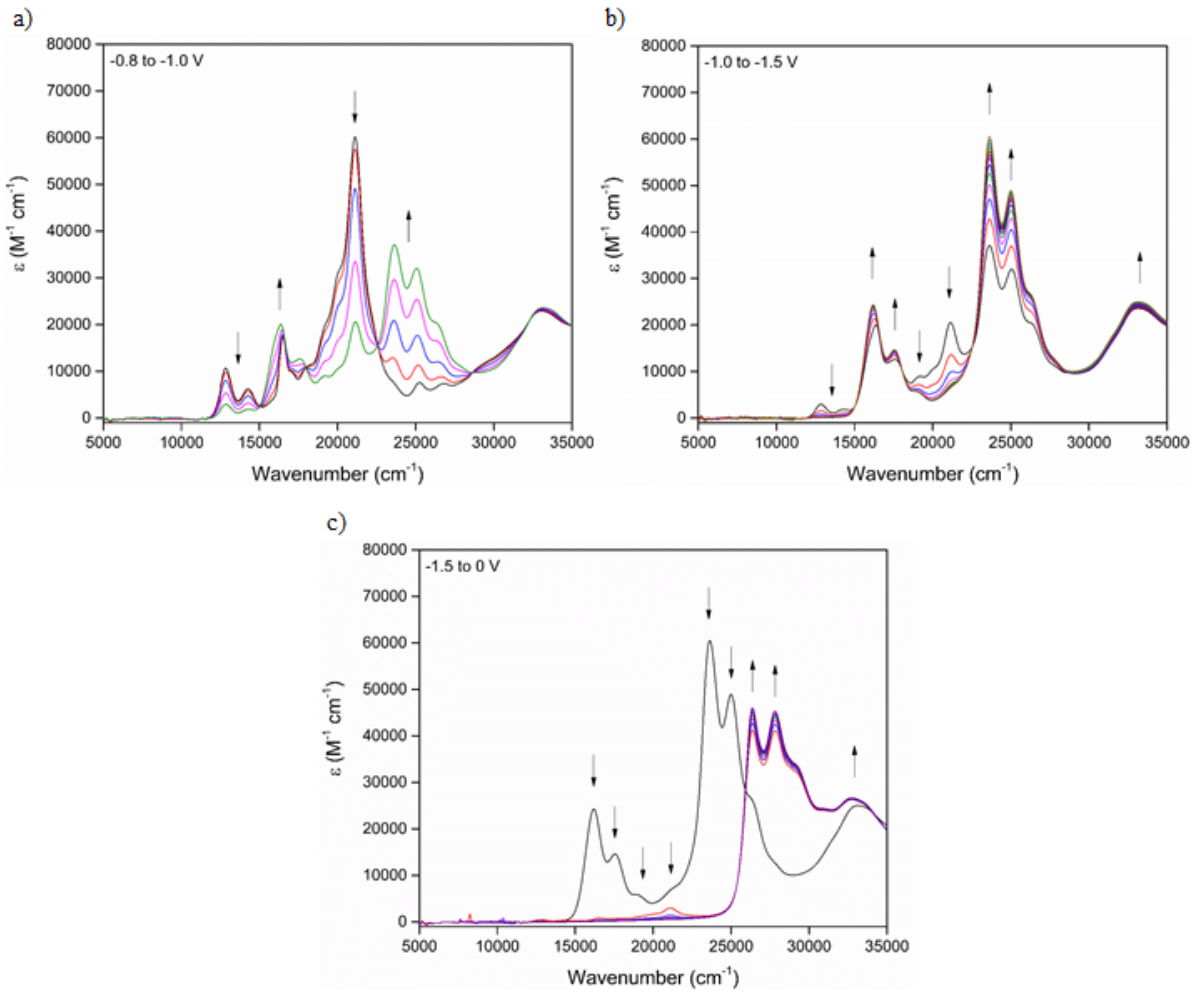

Figure S4. Solution-state UV-Vis-NIR spectroelectrochemistry of the H_4DSNDI ligand in 0.1 M [(*n*-$C_4H_9)_4N]PF_6$/DMF electrolyte over a potential range of a) -0.8 to -1.0 V, b) -1.0 to -1.5 V and c) -1.5 to 0 V showing the formation of the H_4DSNDI dianion and subsequent restoration of the neutral spectrum.

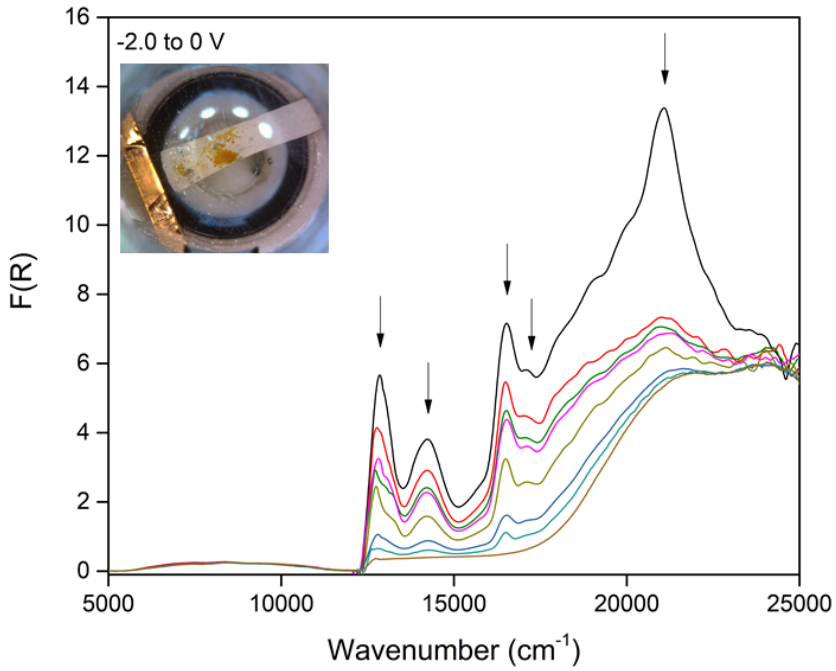

Figure S5. Solid-state UV-Vis-NIR spectroelectrochemistry of **1** in 0.1 M [(*n*-$C_4H_9)_4N]PF_6$/DMF electrolyte showing the restoration of the initial spectrum after potential changes from -2.0 to 0 V where the arrows indicate the direction of the spectral progression. Insert: photograph of the sample acquired at the end of the experiment showing the restoration of the initial colour.

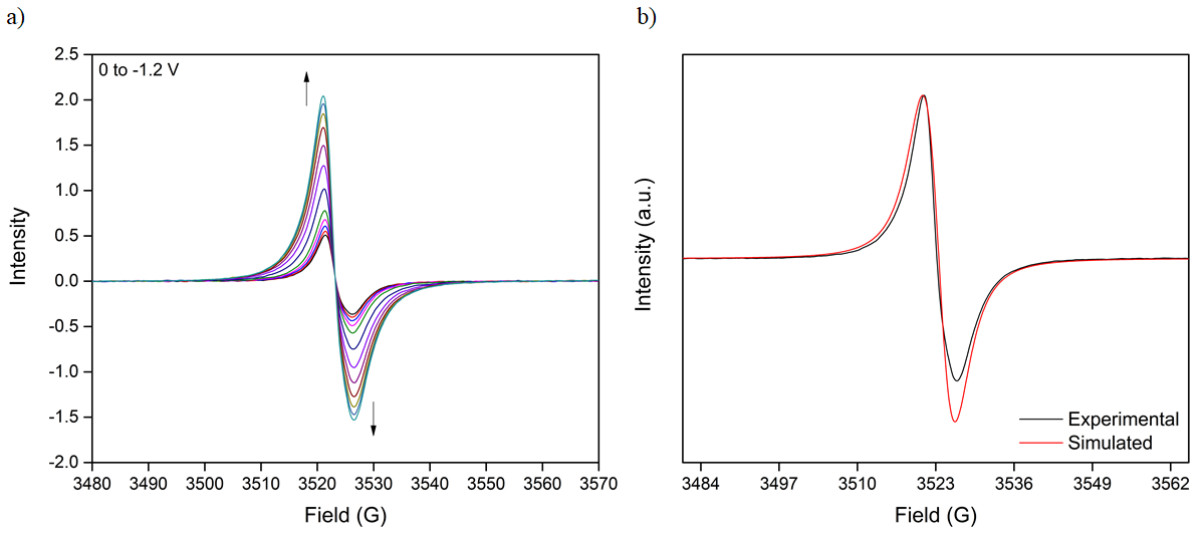

Figure S6. Solid-state EPR spectroelectrochemistry of **1** in 0.1 M [(*n*-$C_4H_9)_4N]PF_6$/DMF electrolyte showing a) potential changes from a) 0 to -1.2 V and b) experimental *vs*. simulated spectra of the EPR signal at -1.2 V using an isotropic model with a simulated *g*-value of 2.0014.

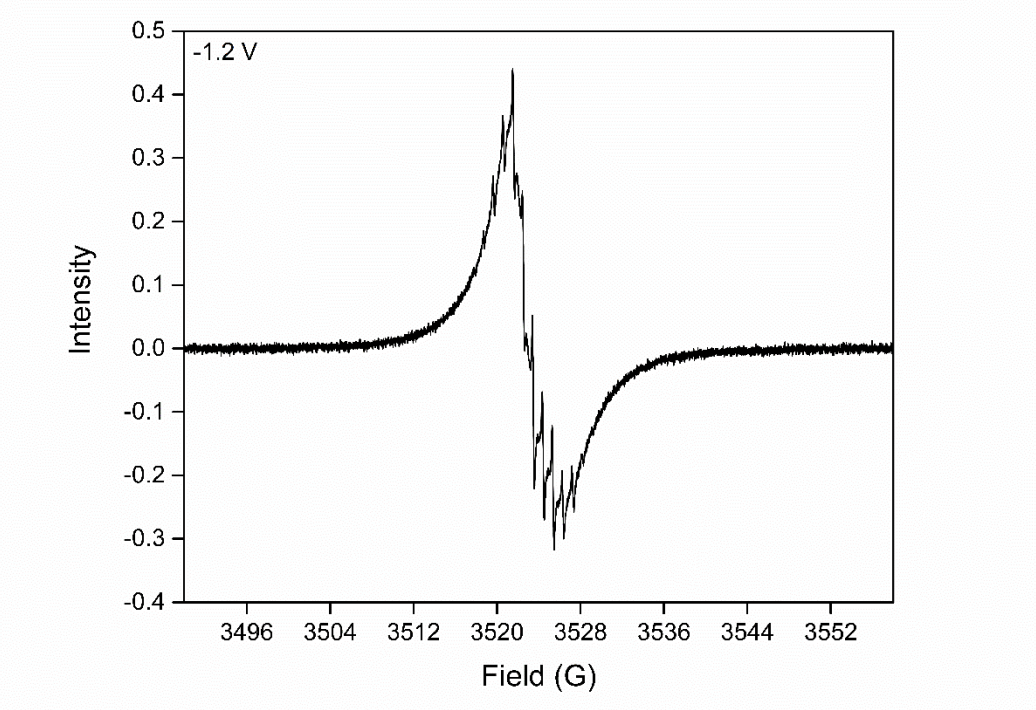

Figure S7. Solid-state EPR spectroelectrochemistry of **1** showing the spectrum at -1.2 V acquired at a modulation amplitude of 0.1 G showing the resolution of the hyperfine splitting of the signal.

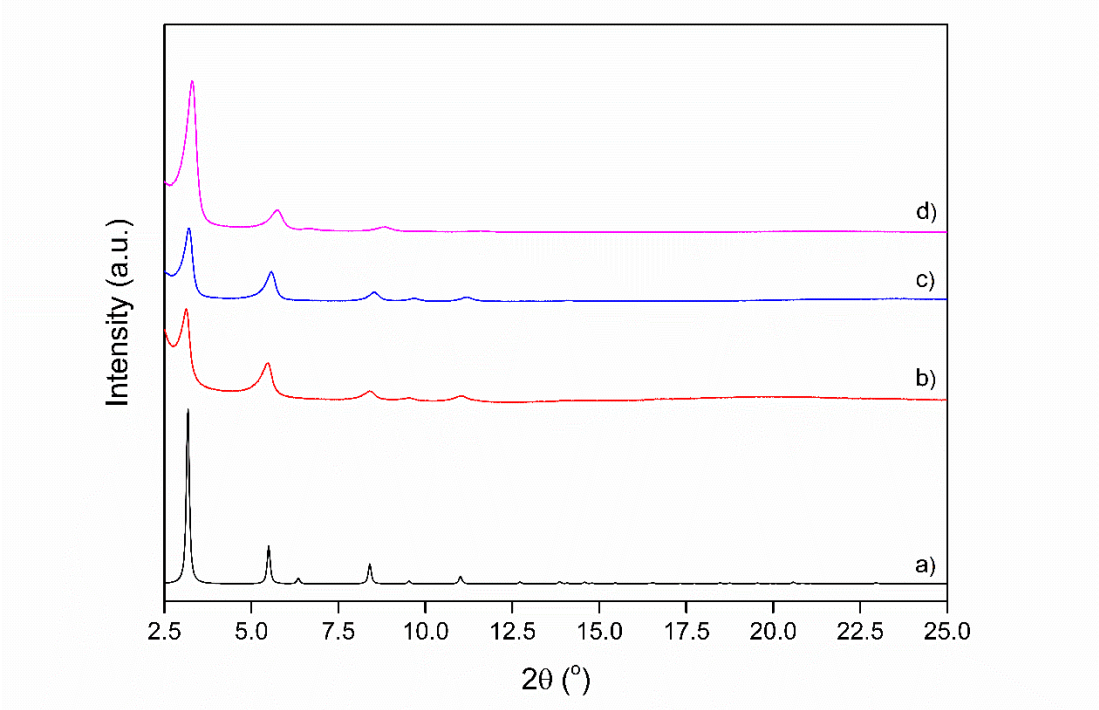

Figure S8. Capillary PXRD patterns of **1** showing a) the predicted pattern, b) the DMF solvated *de novo* phase, c) the MeOH exchanged phase and d) after activation at 80 °C under vacuum.

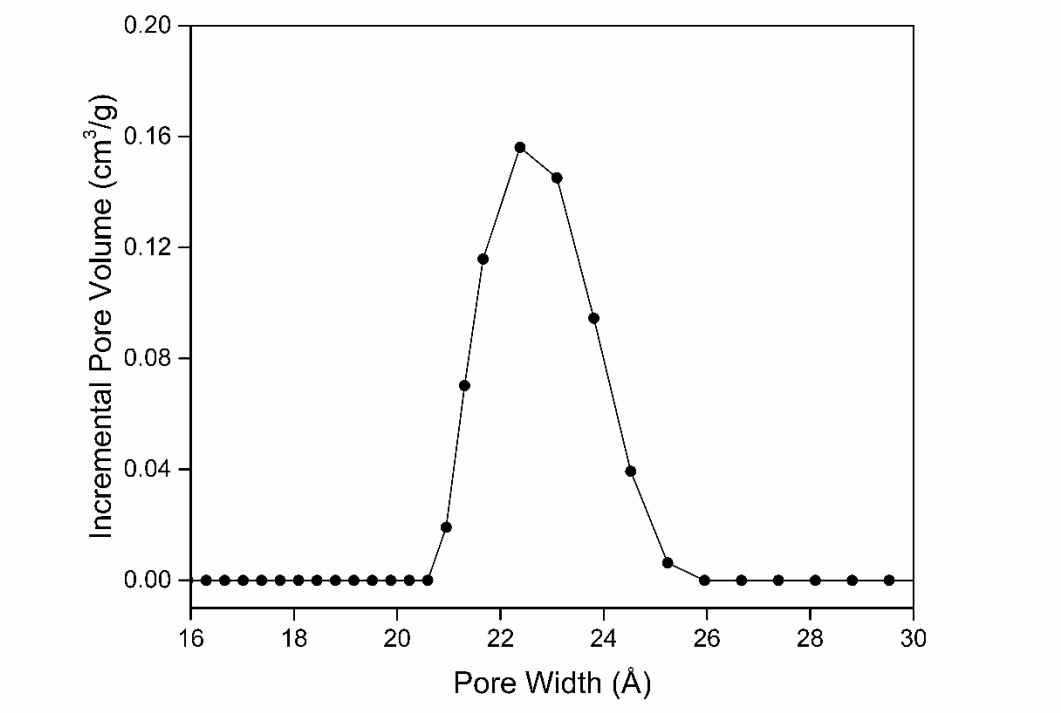

Figure S9. Pore size distribution of activated **1** derived from N_2 gas sorption data at 77 K showing a single pore size of 22.5 Å.

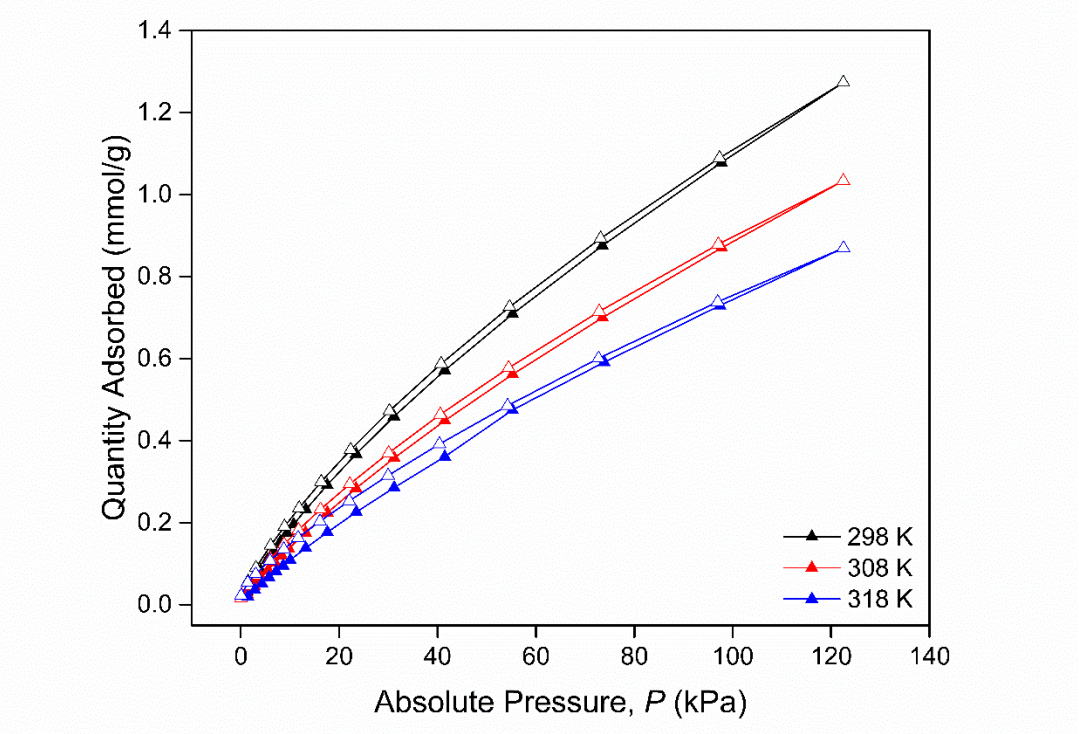

Figure S10. CO_2 sorption (closed triangles) and desorption (open triangles) isotherms of **1** at 298, 308 and 318 K.

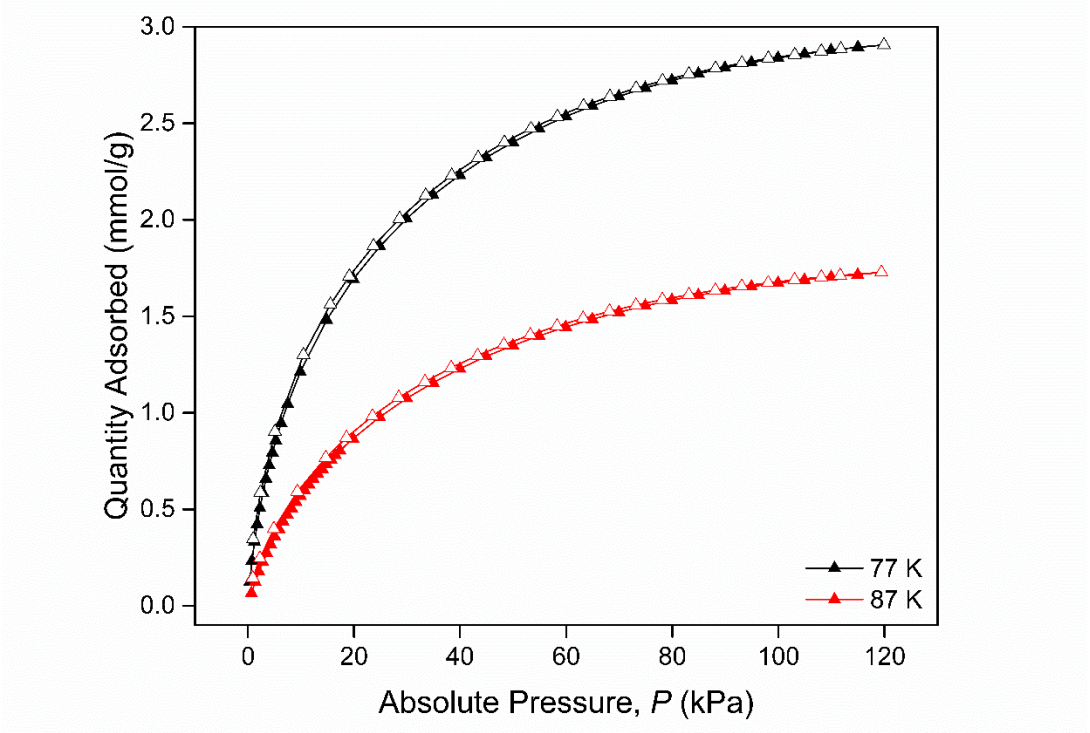

Figure S11. H_2 adsorption (closed triangles) and desorption (open triangles) isotherms of **1** at both 77 and 87 K.

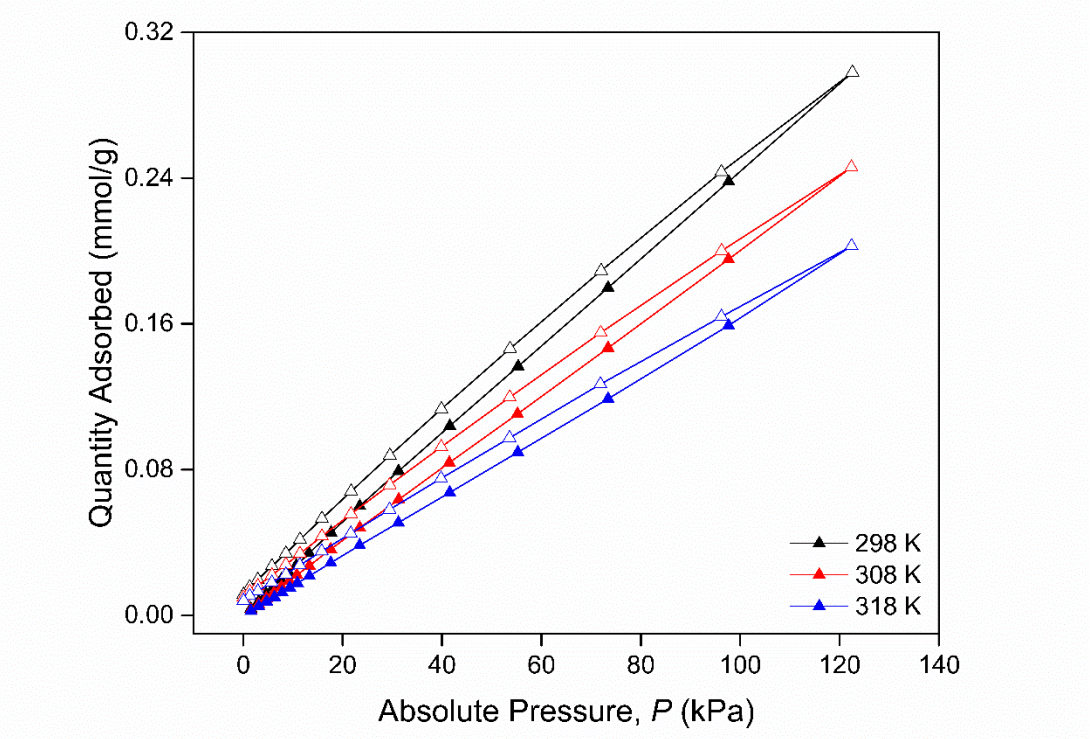

Figure S12. CH_4 sorption (closed triangles) and desorption (open triangles) isotherms of **1** at 298, 308 and 318 K.

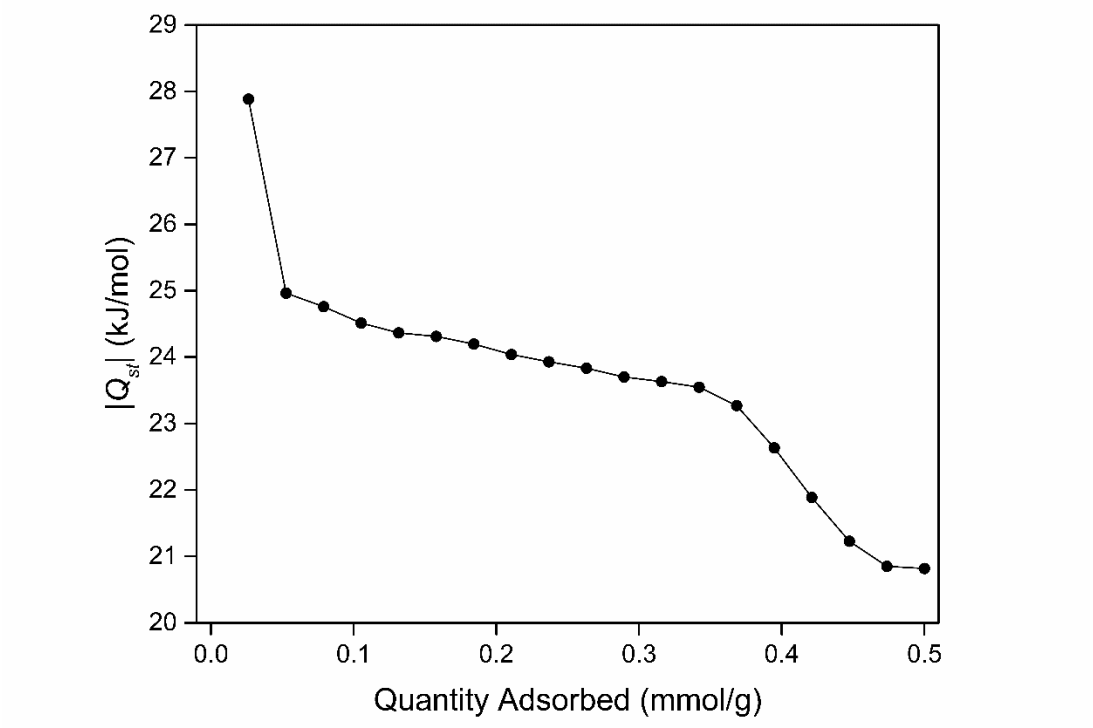

Figure S13. Isosteric heat of adsorption profile of CO_2 calculated from the adsorption isotherms of **1** at 298, 308 and 318 K.

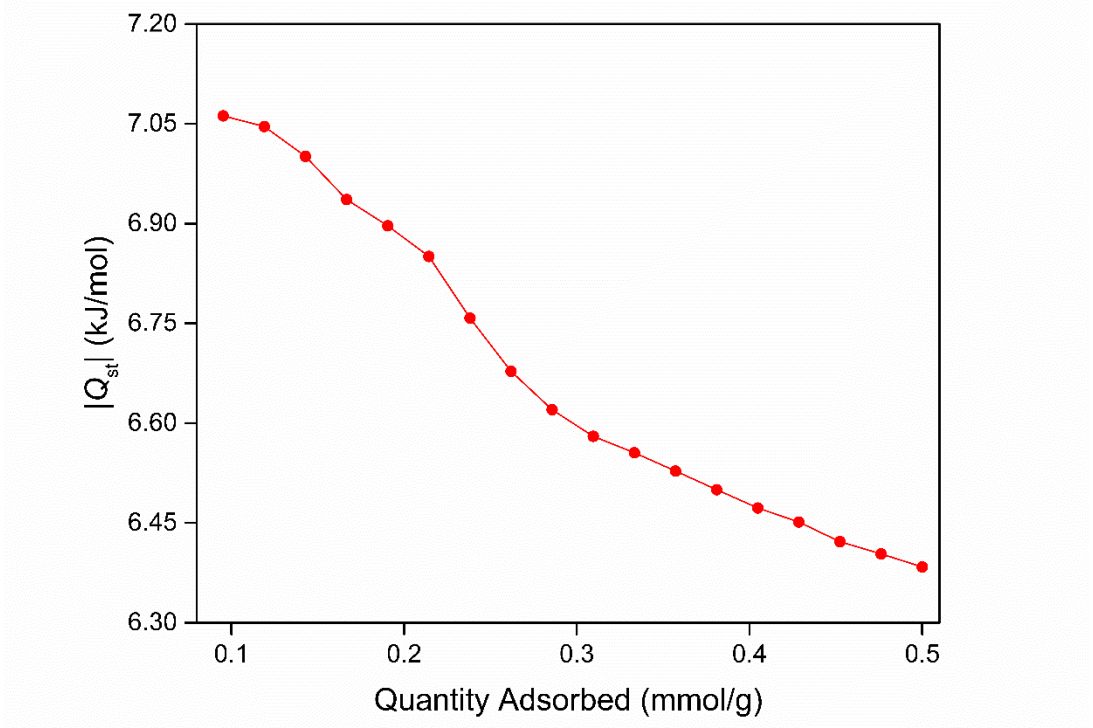

Figure S14. Isosteric heat of adsorption profile of H_2 calculated from the adsorption isotherms of **1** at 77 and 87 K.

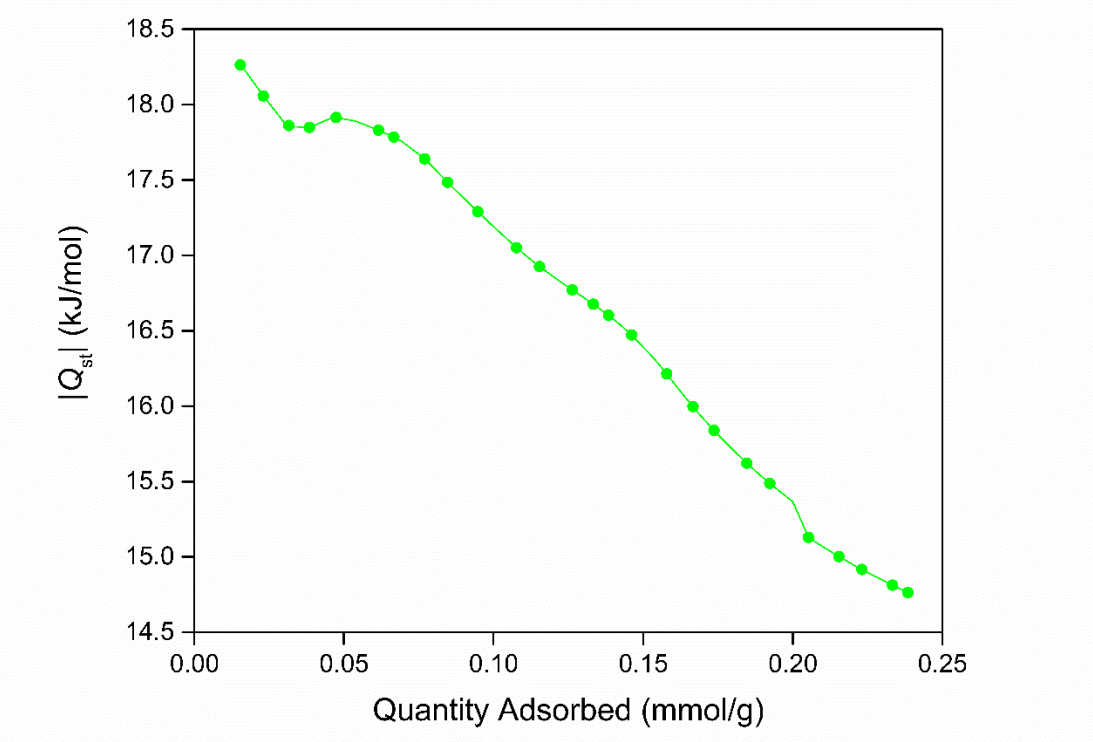

Figure S15. Isosteric heat of adsorption profile of CH_4 calculated from the adsorption isotherms of **1** at 298, 308 and 318 K.

Table S2. H_2, CO_2 and CH_4 uptakes and Q_{st} values of **1**.

Gas	Uptakes (mmol/g)	Q_{st} (kJ/mol)
H_2	2.84†	7.1
CO_2	1.08‡	27.9
CH_4	0.24‡	18.3

† 1 bar at 77 K.

‡ 1 bar at 298 K.

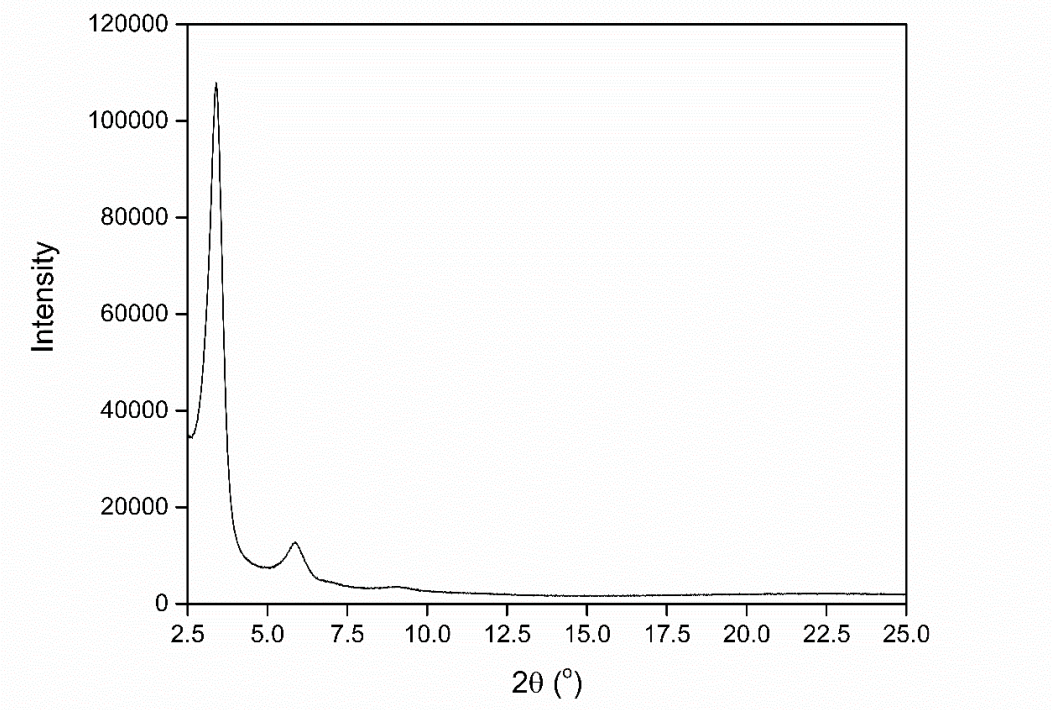

Figure S16. Capillary PXRD of **1** after gas sorption analysis showing retention of structure and crystallinity.

Table S3. Amount of LiNP reductant added to the activated **1** framework and amount of intercalated Li as determined by ICP-MS.

LiNP Reductant Added (Eq)	**Actual Amount of LiNP Reductant (Eq)**	**Li (mol)**	**Zn (mol)**	**Ratio (Li:Zn)**
0.5	0.39	0.903	2.32	1 : 2.57
1.0	0.47	1.16	2.46	1 : 2.12
2.0	1.15	3.12	2.71	1 : 0.87
3.0	1.82	4.04	2.22	1 : 0.55
4.0	2.27	5.95	2.61	1 : 0.44
5.0	2.83	7.23	2.56	1 : 0.35

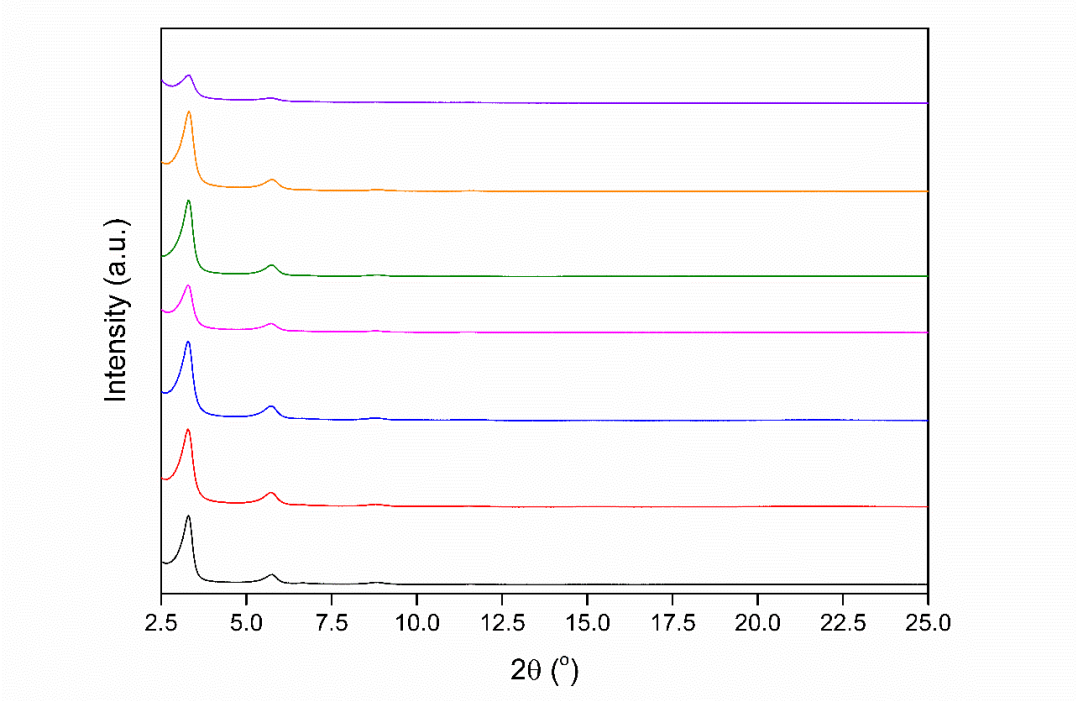

Figure S17. Capillary PXRD of **1** (black) and its reduced analogues generated by chemical reduction with 0.39 (red), 0.47 (blue), 1.15 (brown), 1.82 (green), 2.27 (orange) and 2.83 Eq. (purple) of LiNP.

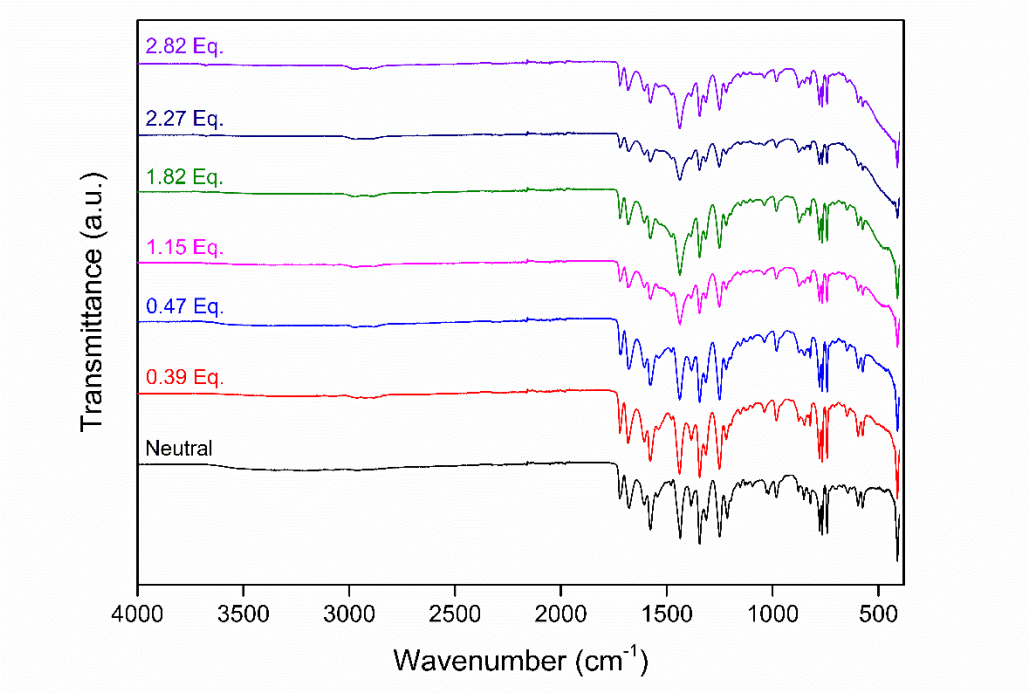

Figure S18. Solid-state IR spectra of **1** and its chemically reduced analogues.

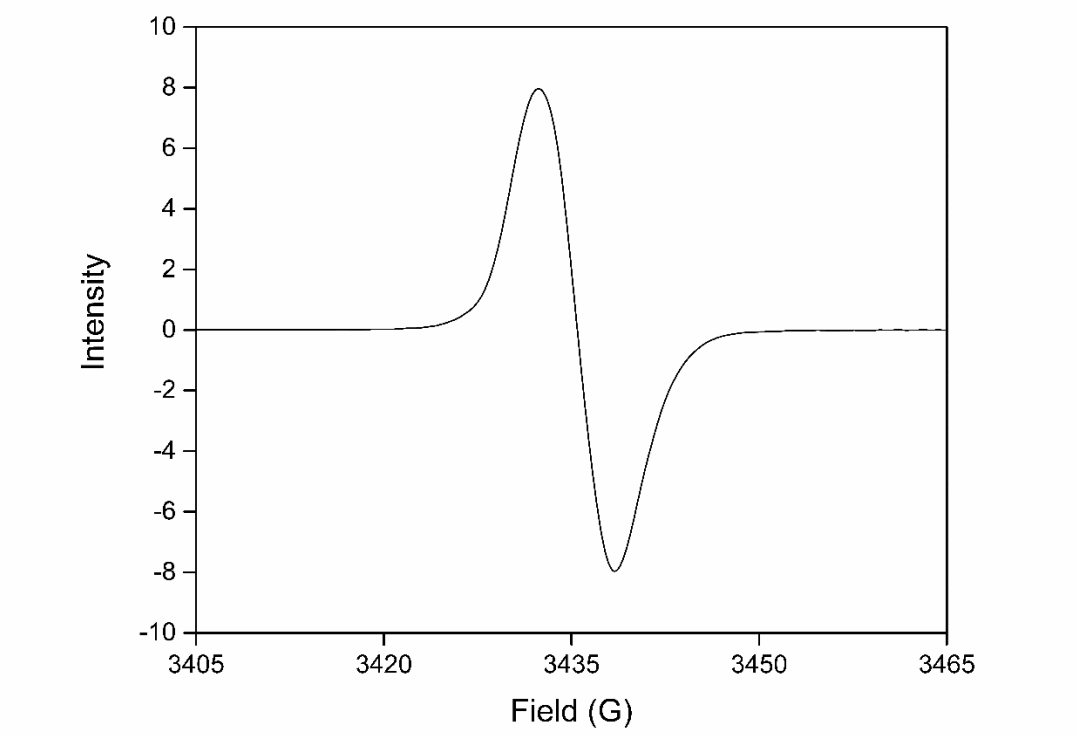

Figure S19. EPR spectrum of **1** chemically reduced by 0.39 Eq. of LiNP.

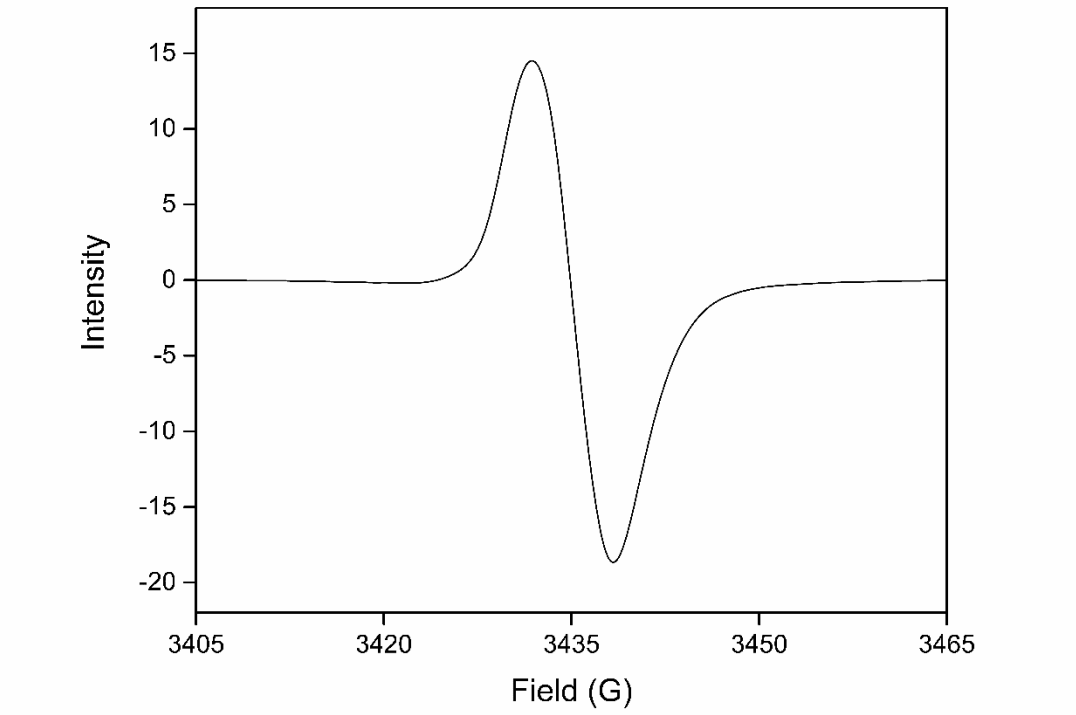

Figure S20. EPR spectrum of **1** chemically reduced by 0.47 Eq. of LiNP.

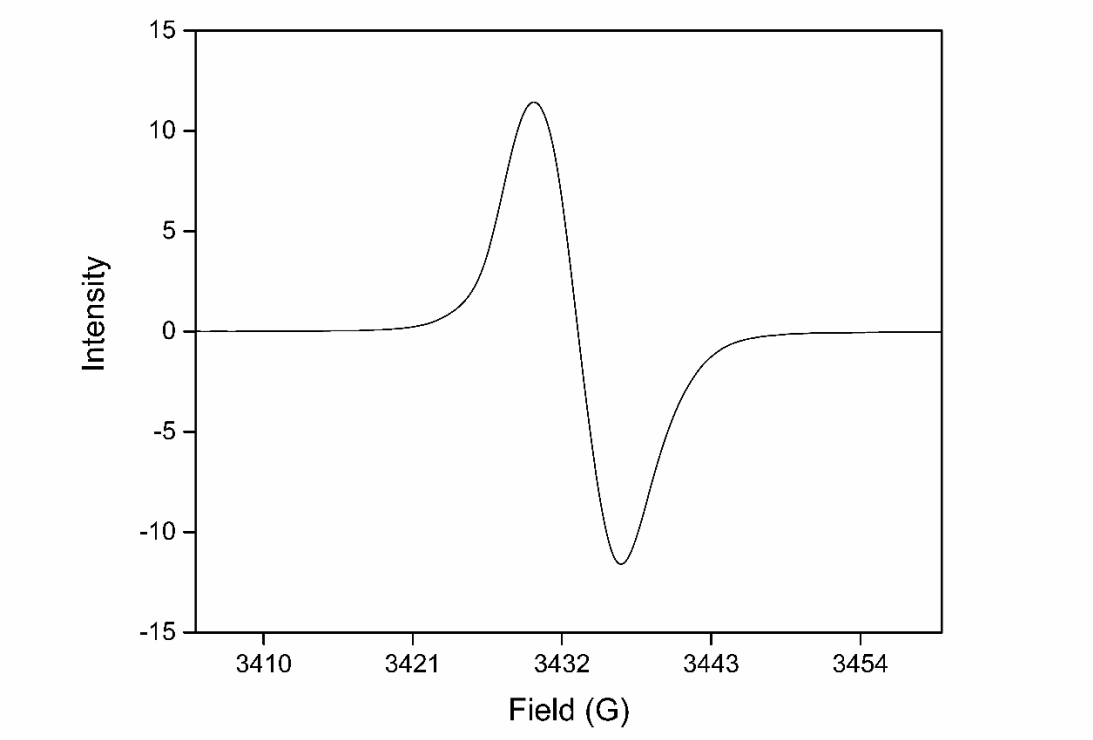

Figure S21. EPR spectrum of **1** chemically reduced by 1.15 Eq. of LiNP.

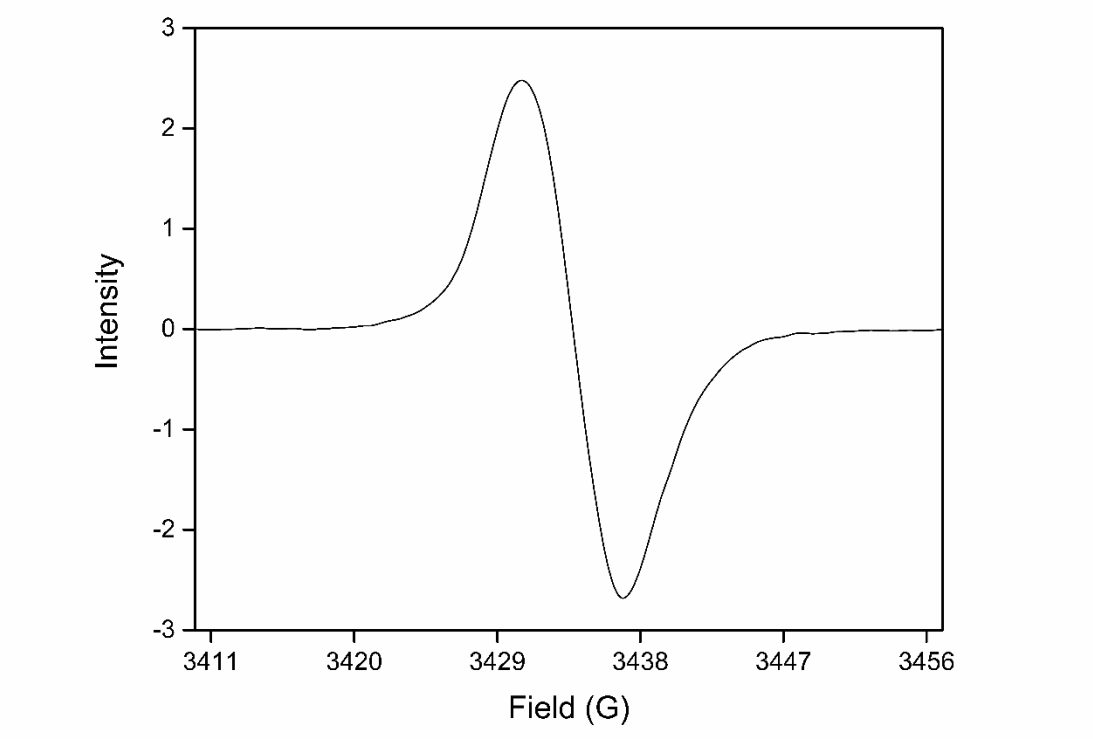

Figure S22. EPR spectrum of **1** chemically reduced by 1.82 Eq. of LiNP.

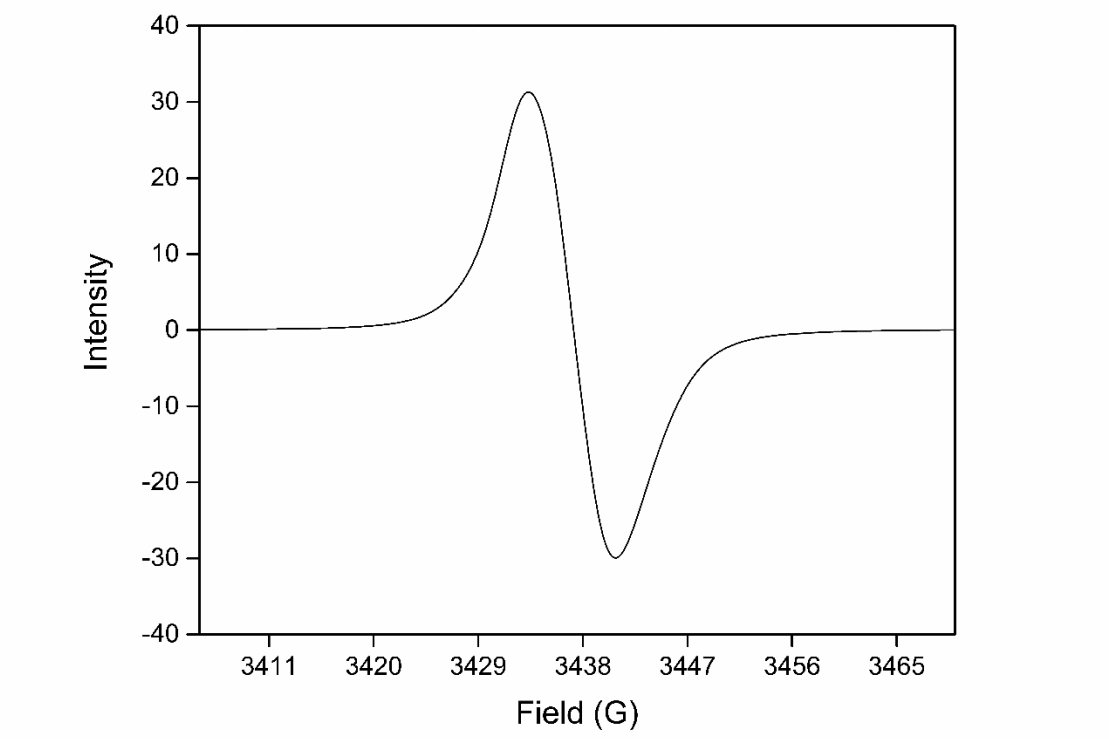

Figure S23. EPR spectrum of **1** chemically reduced by 2.27 Eq. of LiNP.

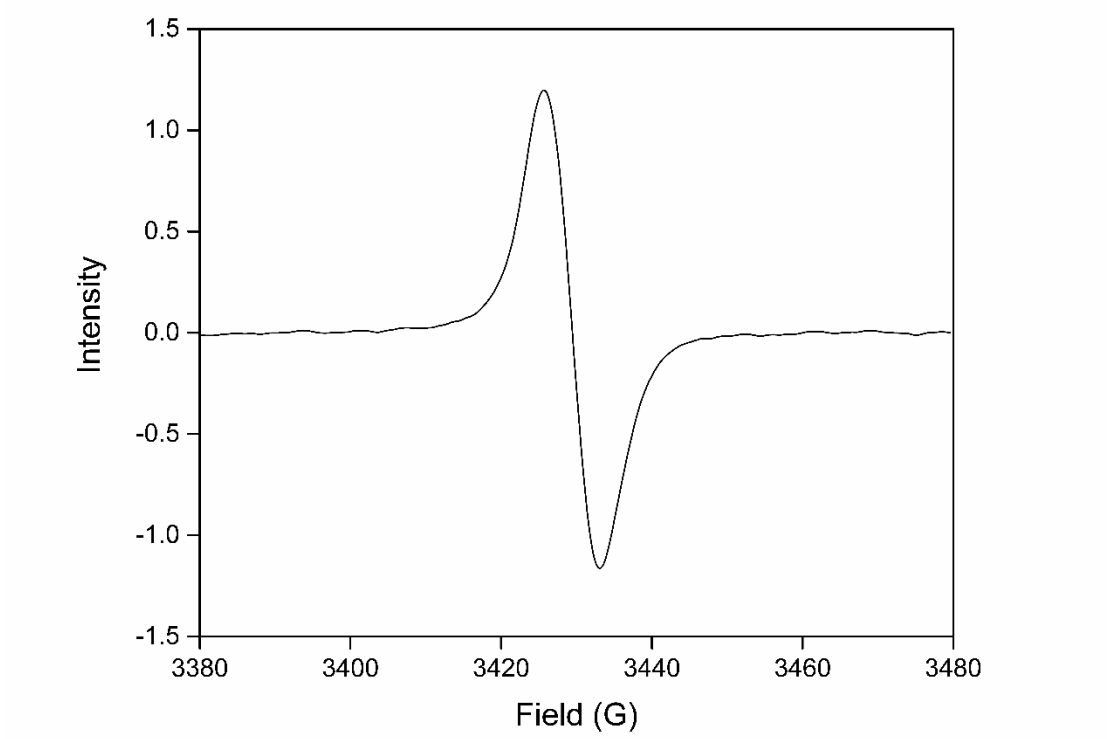

Figure S24. EPR spectrum of **1** chemically reduced by 2.83 Eq. of LiNP.

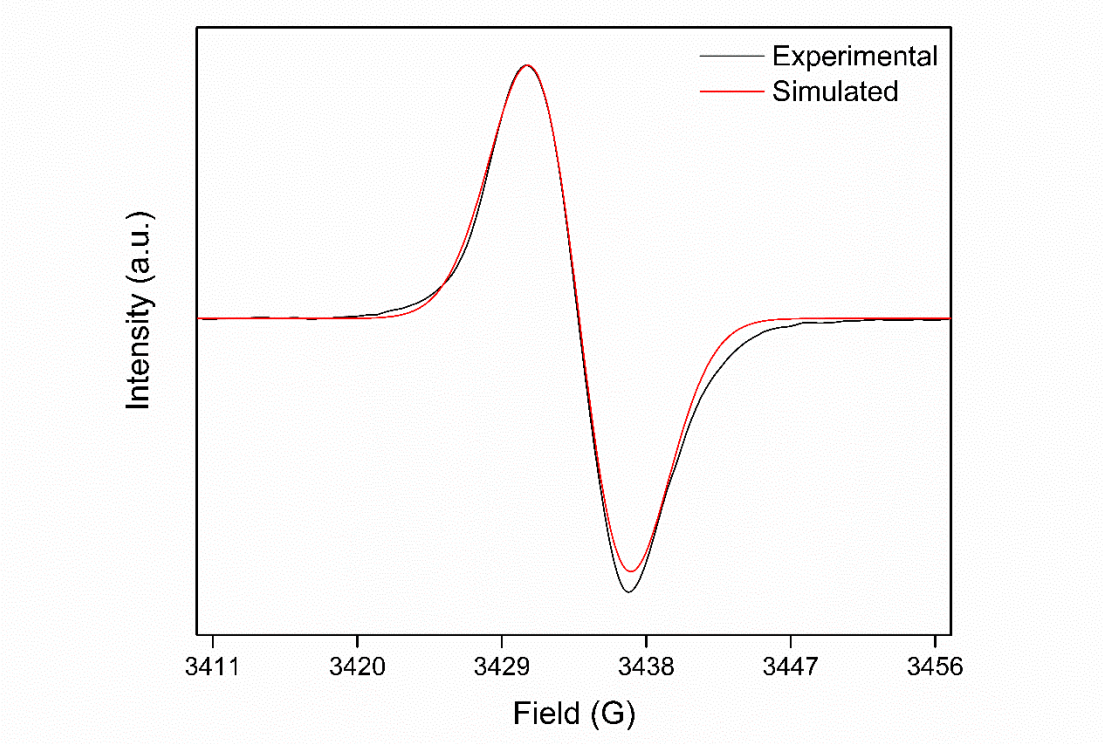

Figure S25. Experimental and simulated spectra of the 1.82 Eq. sample using a simulated *g*-value of 2.0029.

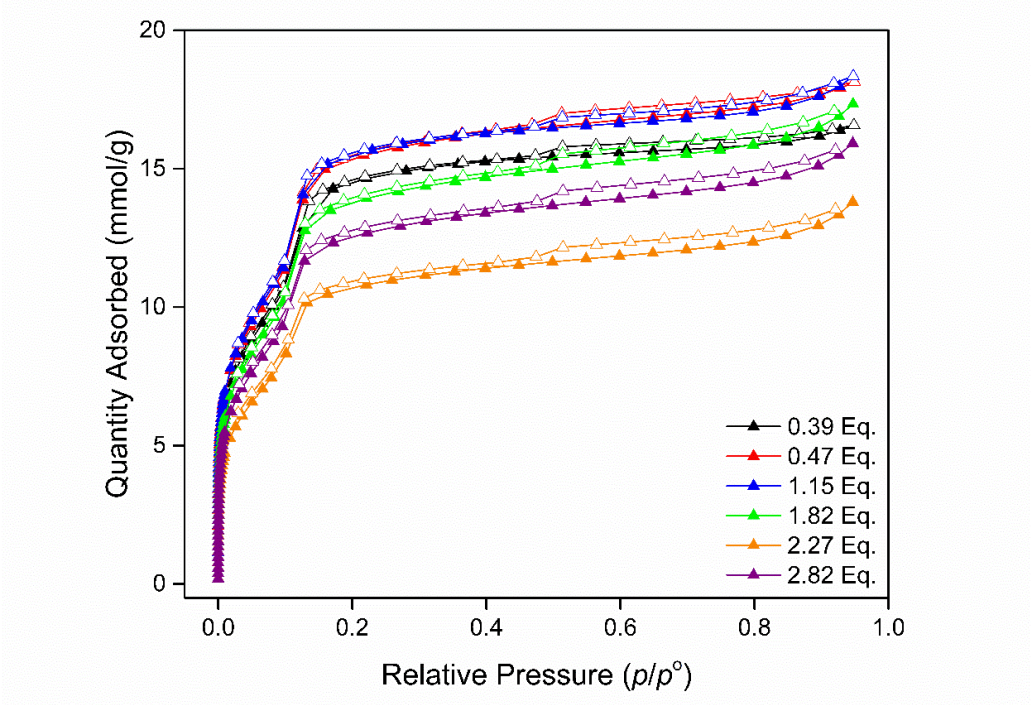

Figure S26. N_2 sorption (closed triangles) and desorption (open triangles) isotherms of the chemically reduced **1** materials at 77 K.

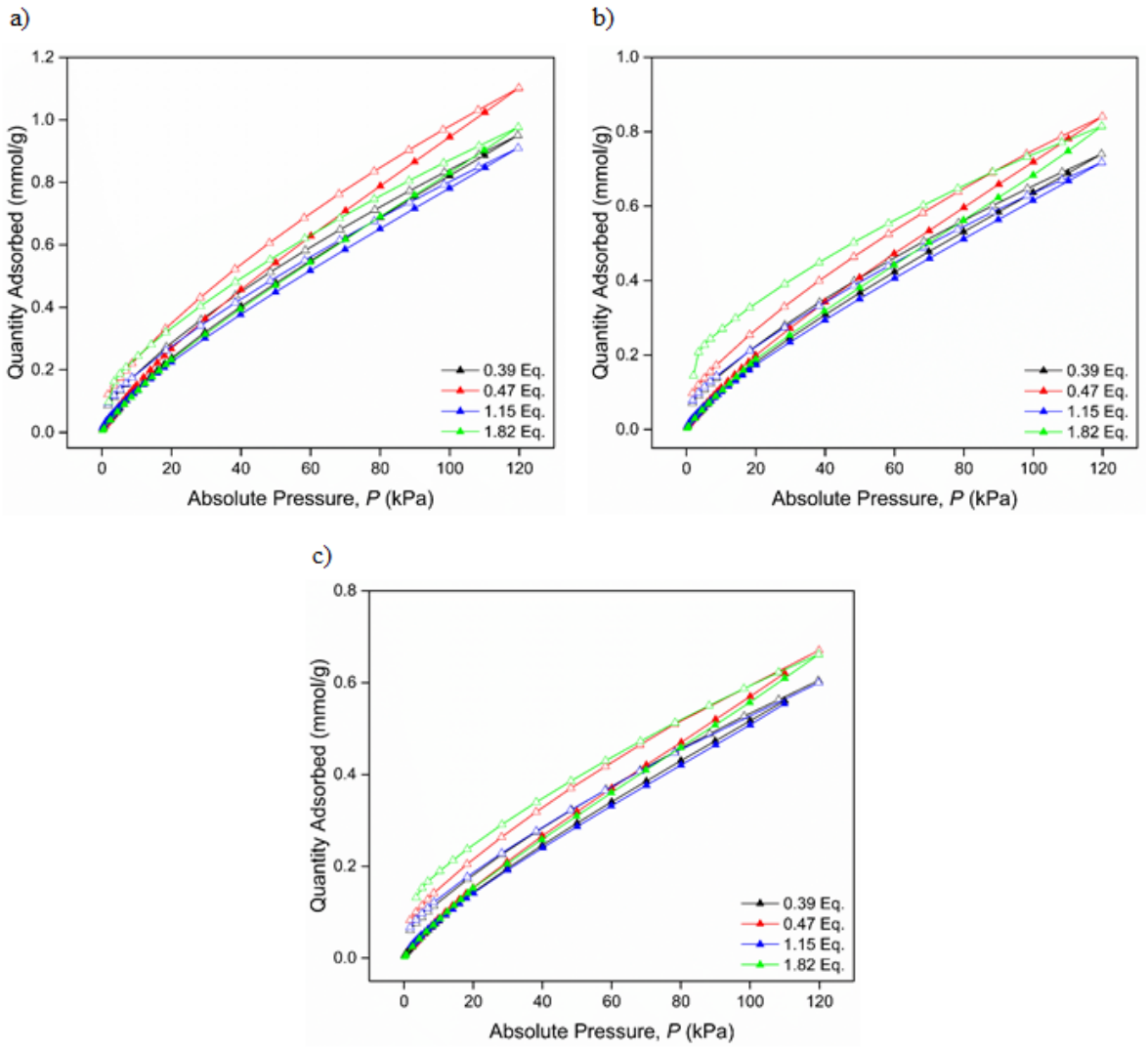

Figure S27. CO_2 sorption (closed triangles) and desorption (open triangles) isotherms of the neutral and chemically reduced **1** materials at a) 298, b) 308 and c) 318 K.

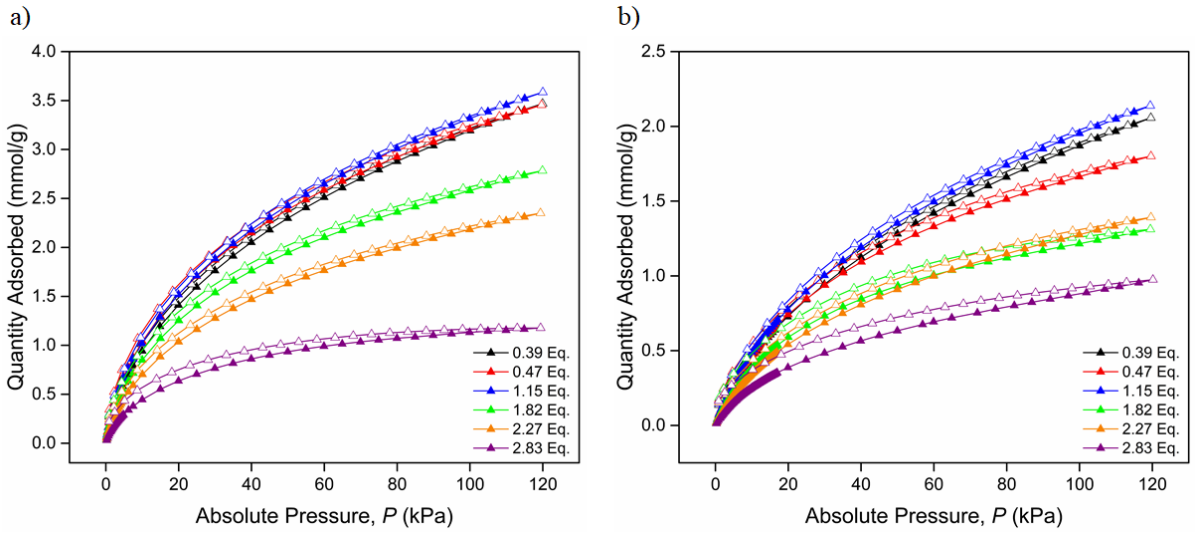

Figure S28. H_2 sorption (closed triangles) and desorption (open triangles) isotherms of the chemically reduced **1** materials at a) 77 and b) 87 K.

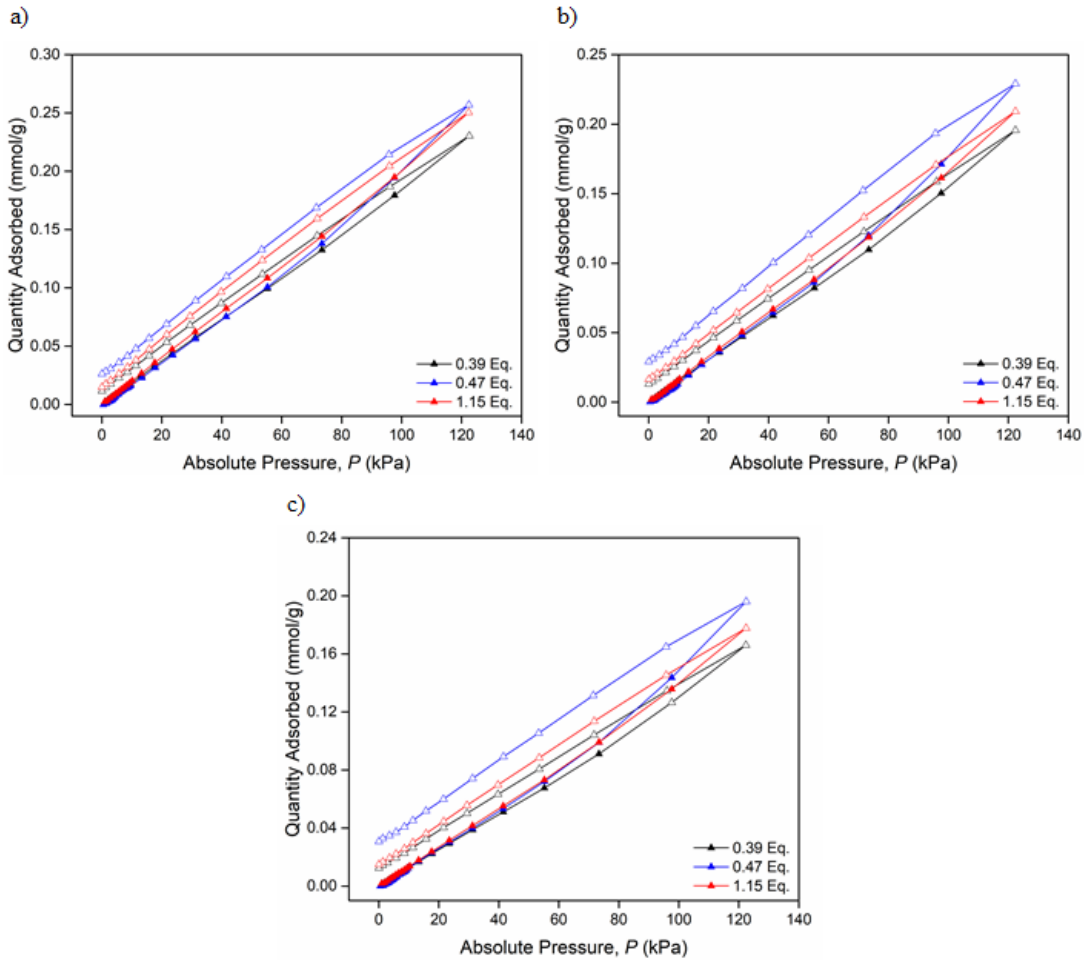

Figure S29. CH_4 sorption (closed triangles) and desorption (open triangles) isotherms of the chemically reduced **1** materials at a) 298, b) 308 and c) 318 K.

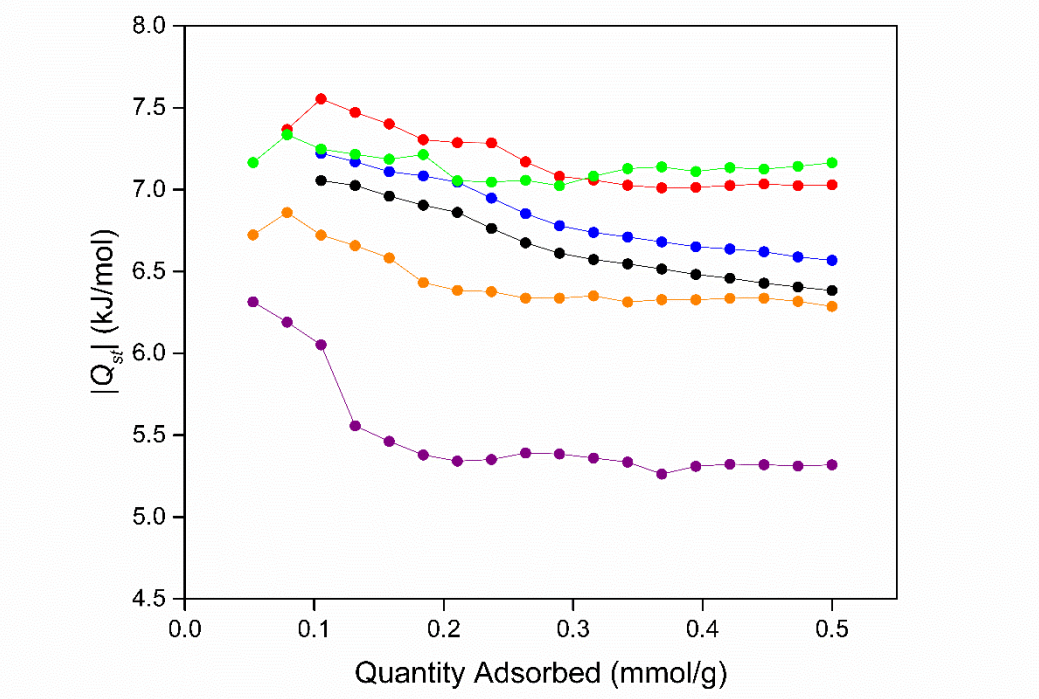

Figure S30. Isosteric heat of adsorption profiles of H_2 calculated from the adsorption isotherms of the **1** chemically reduced by 0.39 (black), 0.47 (red), 1.15 (blue), 1.82 (green), 2.27 (orange) and 2.83 (purple) Eq. of LiNP calculated from adsorption isotherms at 77 and 87 K.

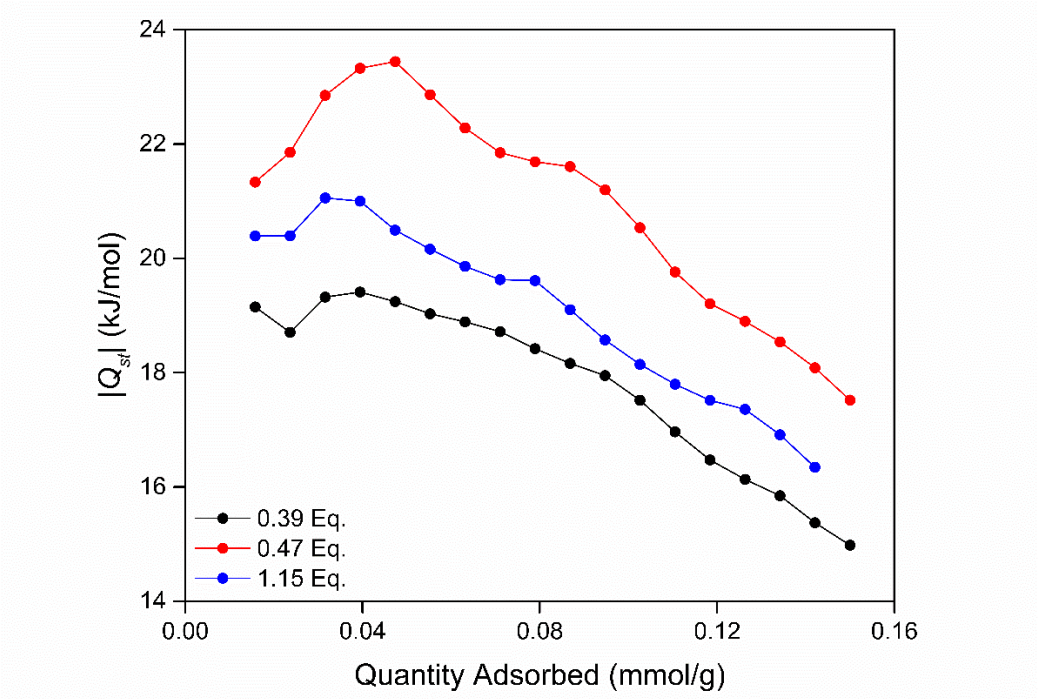

Figure S31. Isosteric heat of adsorption profile of CH_4 calculated from the adsorption isotherms of the reduced analogues of **1** at 298, 308 and 318 K.

Table S4. H_2, CO_2 and CH_4 uptakes and Q_{st} values of the reduced analogues of **1**.

Sample	H_2 Uptake† (mmol/g)	H_2 Q_{st} (kJ/mol)	CO_2 Uptake‡ (mmol/g)	CO_2 Q_{st} (kJ/mol)	CH_4 Uptake‡ (mmol/g)	CH_4 Q_{st} (kJ/mol)
0.39 Eq.	3.19	7.06	0.82	25.5	0.18	19.1
0.47 Eq.	3.21	7.56	0.95	29.5	0.20	21.3
1.15 Eq.	3.31	7.22	0.78	44.9	0.20	20.4
1.82 Eq.	2.58	7.16	0.83	22.7		
2.27 Eq.	2.19	6.72				
2.83 Eq.	1.13	6.31				

† 1 bar at 77 K.

‡ 1 bar at 298 K.

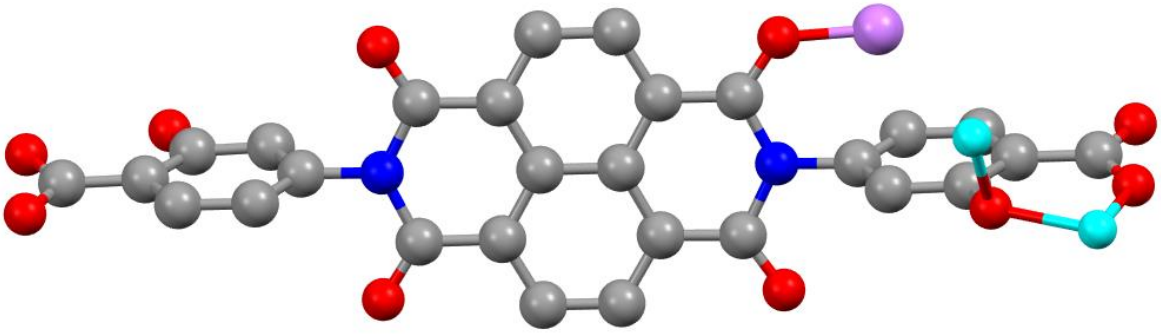

Figure S32. Snapshot of simulated Zn_2(DSNDI) structure (cleaved from the periodic DFT optimised structure) showing the calculated position of the Li^+ cation after chemical reduction. Atom labelling: Zn = turquoise, O = red, N = blue, C = grey and Li = mauve.

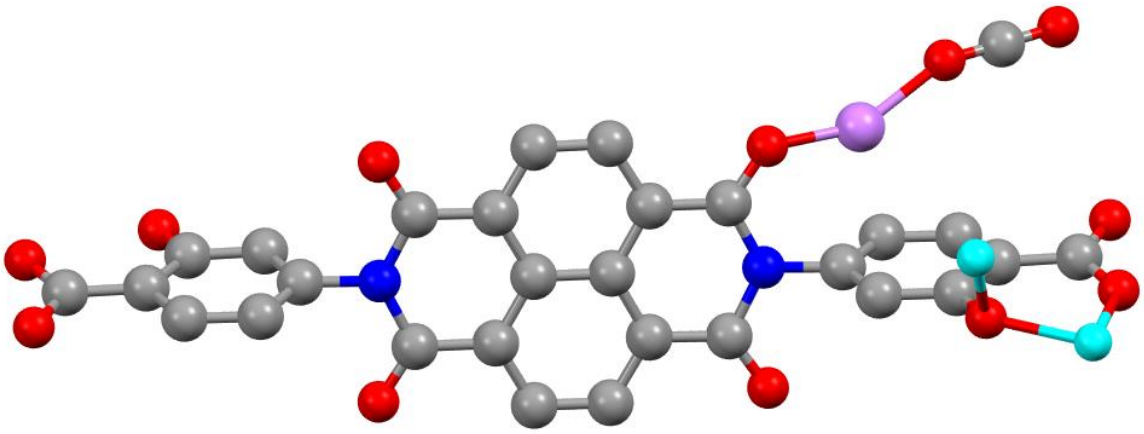

Figure S33. Snapshot of simulated Zn_2(DSNDI) structure (cleaved from the periodic DFT optimised structure) showing the calculated positions of the Li^+ cation after chemical reduction and its interaction with CO_2 guests. Atom labelling: Zn = turquoise, O = red, N = blue, C = grey and Li = mauve.

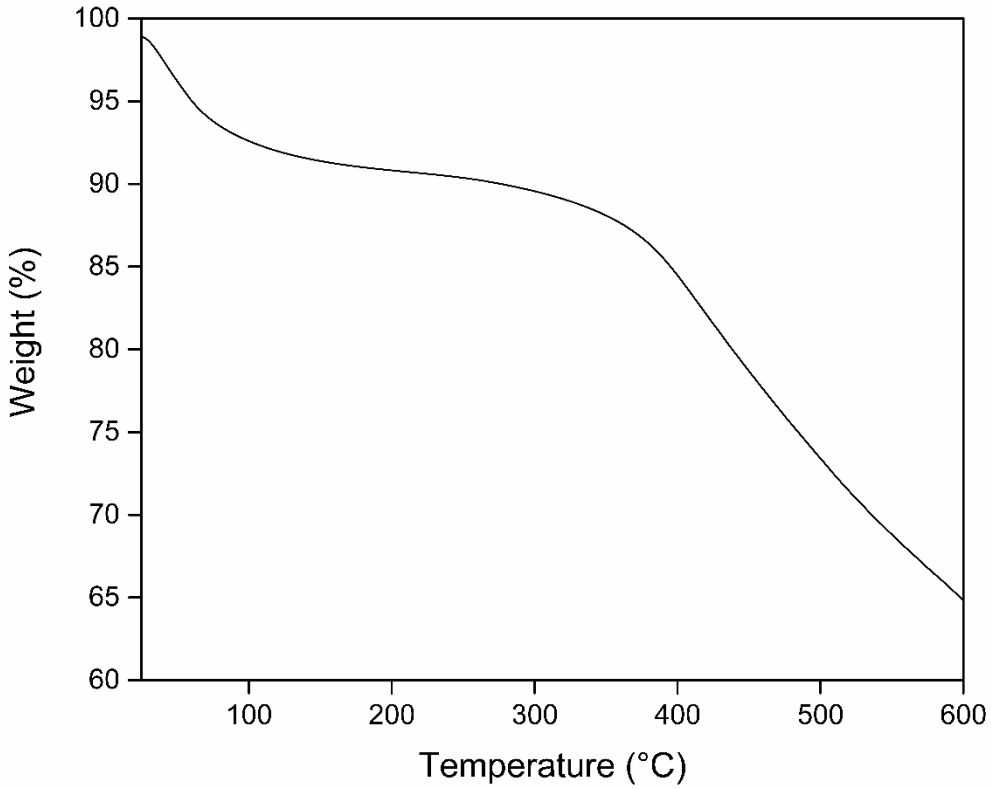

Figure S34. Thermal gravimetric analysis of **1** from 25-600 °C at 2 °C min^{-1}.

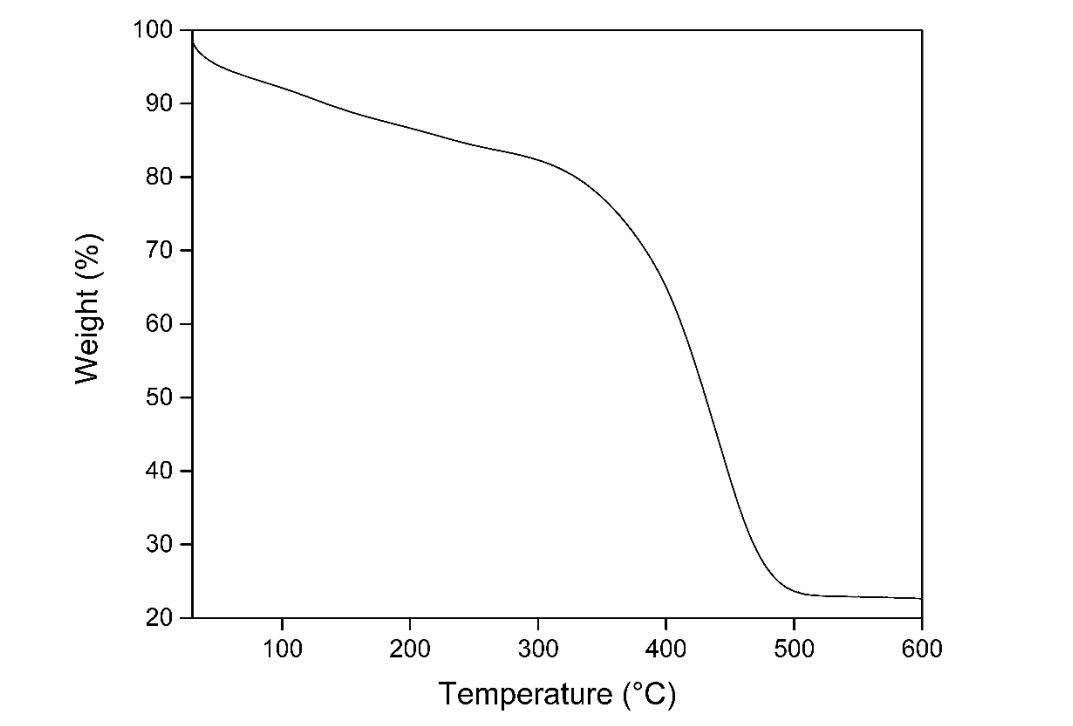

Figure S35. Thermal gravimetric analysis of **1** chemically reduced by 0.39 Eq. of LiNP from 30-600 °C at 2 °C min^{-1}.

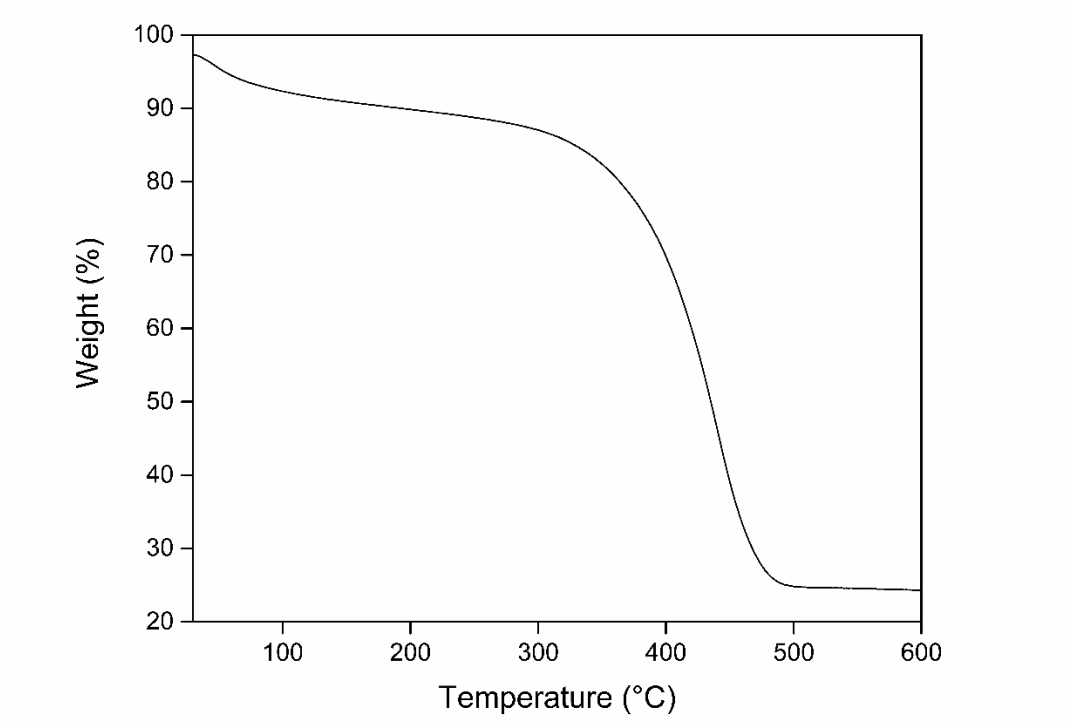

Figure S36. Thermal gravimetric analysis of **1** chemically reduced by 0.47 Eq. of LiNP from 30-600 °C at 2 °C min^{-1}.

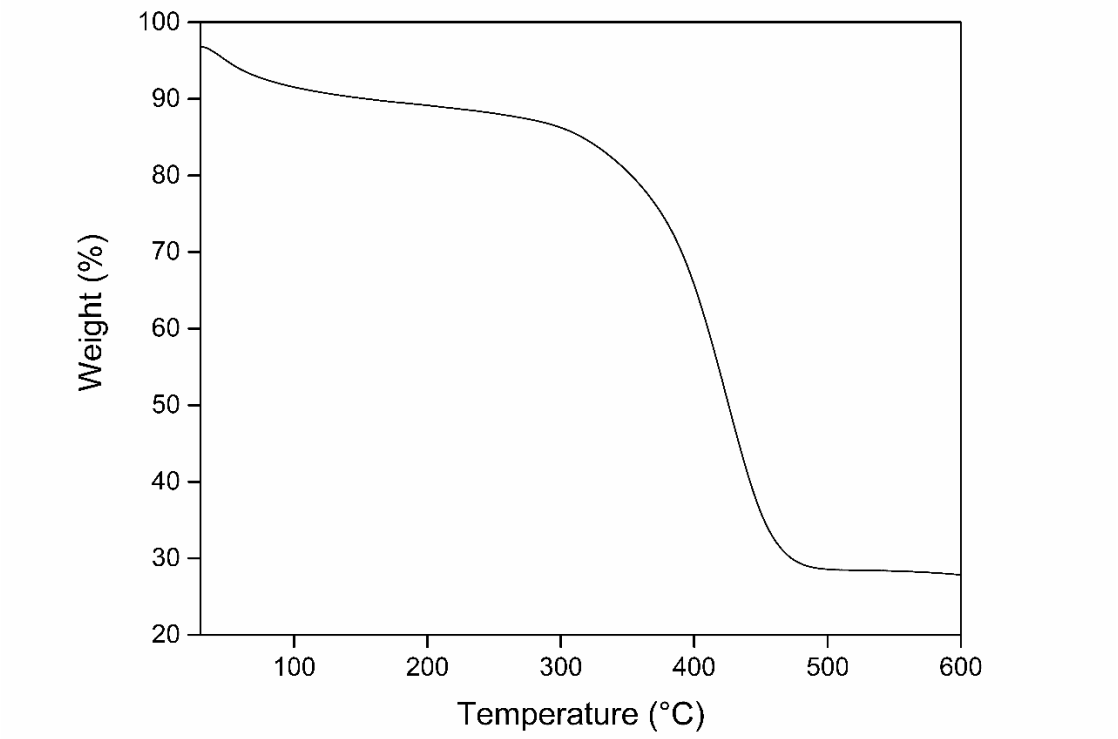

Figure S37. Thermal gravimetric analysis of **1** chemically reduced by 1.15 Eq. of LiNP from 30-600 °C at 2 °C min^{-1}.

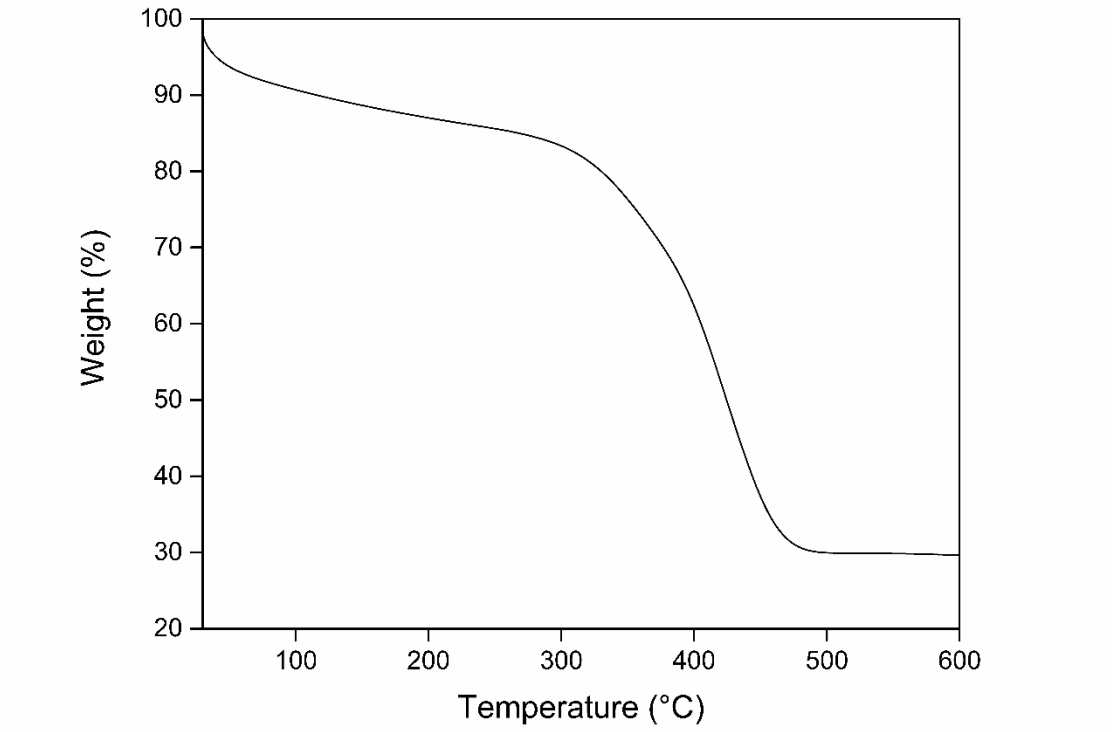

Figure S38. Thermal gravimetric analysis of **1** chemically reduced by 1.82 Eq. of LiNP from 30-600 °C at 2 °C min^{-1}.

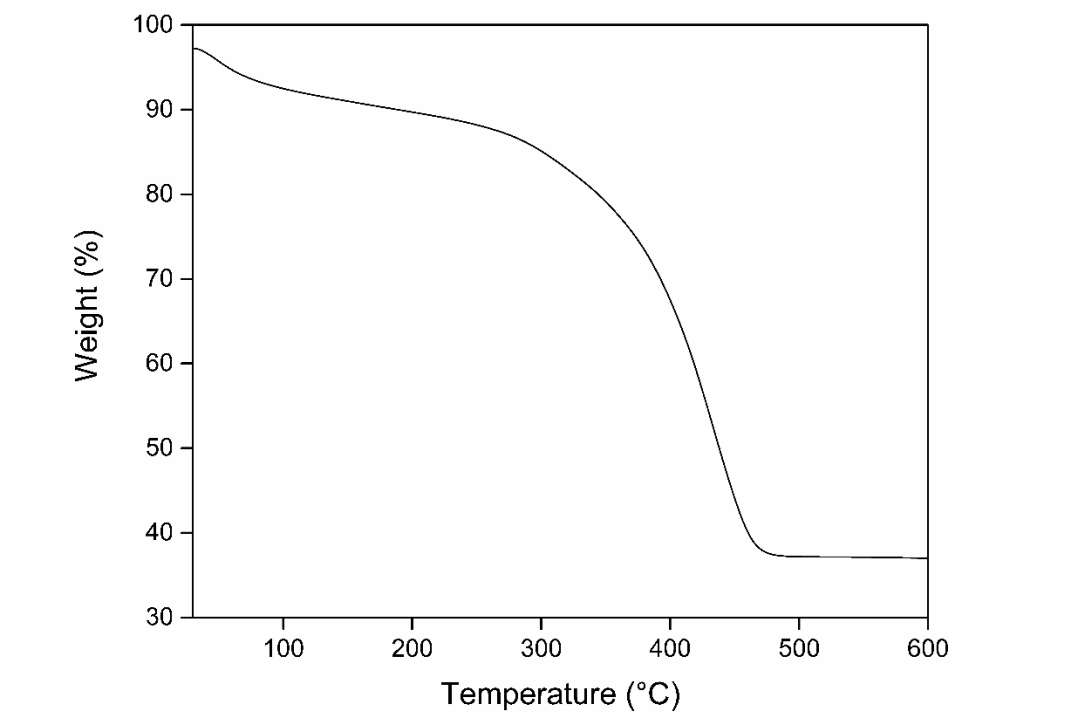

Figure S39. Thermal gravimetric analysis of **1** chemically reduced by 2.27 Eq. of LiNP from 30-600 °C at 2 °C min^{-1}.

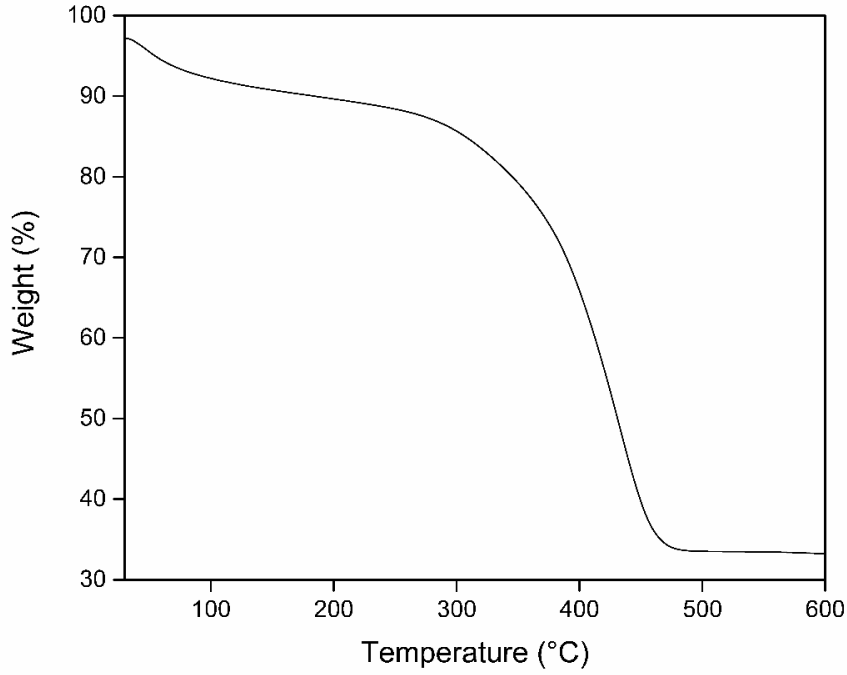

Figure S40. Thermal gravimetric analysis of **1** chemically reduced by 2.83 Eq. of LiNP from 30-600 °C at 2 °C min^{-1}.

References

1. Guo, Z.; Panda, D. K.; Gordillo, M. A.; Khatun, A.; Wu, H.; Zhou, W.; Saha, S. *ACS Appl. Mater. Interfaces* **2017**, *9*, 32413-32417.
2. Rigaku Oxford Diffraction, Yarnton, Oxfordshire, England, 2014.
3. Technologies, A. Agilent Technologies Ltd, Yarnton, Oxfordshire, England, 2011-2013.
4. Sheldrick, G. *Acta Cryst.* **2015**, *A71*, 3-8.
5. Sheldrick, G. *Acta Cryst.* **2015**, *C71*, 3-8.
6. Hubschle, C. B.; Sheldrick, G. M.; Dittrich, B. *J. App. Cryst.* **2011**, *44*, 1281-1284.
7. Murray, P. R.; Collison, D.; Daff, S.; Austin, N.; Edge, R.; Flynn, B. W.; Jack, L.; Leroux, F.; McInnes, E. J. L.; Murray, A. F.; Sells, D.; Stevenson, T.; Wolowska, J.; Yellowlees, L. J. *J. Magn. Reson.* **2011**, *213*, 206-209.
8. Hua, C.; Baldansuren, A.; Tuna, F.; Collison, D.; D'Alessandro, D. M. *Inorg. Chem.* **2016**, *55*, 7270-7280.
9. Hua, C.; Doheny, P. W.; Ding, B.; Chan, B.; Yu, M.; Kepert, C. J.; D'Alessandro, D. M. *J. Am. Chem. Soc.* **2018**, *140*, 6622-6630.
10. Stoll, S.; Schweiger, A. *J. Magn. Reson.* **2006**, *178*, 42-55.
11. Dassault Systèmes BIOVIA, Material Studio, San Diego: Dassault Systèmes, 2019.
12. A. K. Rappe, C. J. Casewit, K. S. Colwell, W. A. Goddard, and W. M. Skiff, *J. Am. Chem. Soc.* **1992**, *114*, 10024-10035.
13. Kresse, G.; Hafner, J.. *Phys. Rev. B* **1993**, *48*, 13115-13118.
14. Grimme, S.; Ehrlich, S.; Goerigk, L. *J. Comp. Chem.* **2011**, *32*, 1456-1465.
15. Perdew, J. P.; Burke, K.; Ernzerhof, M. *Phys. Rev. Lett.* **1996**, *77*, 3865-3868.
16. Kresse, G.; Joubert, D. *Phys. Rev. B* **1999**, *59*, 1758-1775.